

# Convergent Genetic Adaptation in Human Tumors Developed Under Systemic Hypoxia and in Populations Living at High Altitudes



Carlota Arenillas<sup>1,2,3</sup>, Lucía Celada<sup>4,5</sup>, José Ruiz-Cantador<sup>6</sup>, Bruna Calsina<sup>7</sup>, Debayan Datta<sup>1</sup>, Eduardo García-Galea<sup>8</sup>, Roberta Fasani<sup>9</sup>, Ana Belén Moreno-Cárdenas<sup>1</sup>, Juan José Alba-Linares<sup>4,5,10,11,12</sup>, Berta Miranda-Barrio<sup>3,13,14,15</sup>, Ángel M. Martínez-Montes<sup>7</sup>, Cristina Alvarez-Escola<sup>16</sup>, Beatriz Lecumberri<sup>16</sup>, Ana González García<sup>6</sup>, Shahida K. Flores<sup>17</sup>, Emmanuel Esquivel<sup>17</sup>, Yanli Ding<sup>18</sup>, Mirko Peitzsch<sup>19</sup>, José-Ángel Robles-Guirado<sup>20</sup>, Rita Maria Regojo Zapata<sup>21</sup>, José Juan Pozo-Kreilinger<sup>21</sup>, Carmela Iglesias<sup>22</sup>, Trisha Dwight<sup>23,24</sup>, Christopher A. Muir<sup>25,26</sup>, Amelia Oleaga<sup>27</sup>, María Elvira Garrido-Lestache Rodríguez-Monte<sup>28</sup>, María Jesús Del Cerro<sup>28</sup>, Isaac Martínez-Bendayán<sup>29</sup>, Enol Álvarez-González<sup>4,5,30</sup>, Tamara Cubiella<sup>4,5</sup>, Delmar Muniz Lourenço Jr<sup>31</sup>, Maria Adelaide A. Pereira<sup>31</sup>, Nelly Burnichon<sup>32,33</sup>, Alexandre Buffet<sup>32,33</sup>, Craig Broberg<sup>34</sup>, Paxton V. Dickson<sup>35</sup>, Mario F. Fraga<sup>4,5,10,11,12</sup>, José Luis Llorente Pendás<sup>2,4,36</sup>, Joaquín Rueda Soriano<sup>14,37</sup>, Francisco Buendía Fuentes<sup>14,37</sup>, Sergio P.A. Toledo<sup>38</sup>, Roderick Clifton-Bligh<sup>39</sup>, Rodrigo Dienstmann<sup>8,50</sup>, Josep Villanueva<sup>20</sup>, Jaime Capdevila<sup>40,41</sup>, Anne-Paule Gimenez-Roqueplo<sup>32,33</sup>, Judith Favier<sup>33</sup>, Paolo Nuciforo<sup>9</sup>, William F. Young Jr<sup>42</sup>, Nicole Bechmann<sup>19</sup>, Alexander R. Opatowsky<sup>43,44</sup>, Anand Vaidya<sup>45</sup>, Irina Bancos<sup>42</sup>, Donatè Weghorn<sup>46</sup>, Mercedes Robledo<sup>7,42</sup>, Anna Casteràs<sup>3,47</sup>, Laura Dos-Subirà<sup>13,14,15</sup>, Igor Adameyko<sup>48,49</sup>, María-Dolores Chiara<sup>4,5</sup>, Patricia L.M. Dahia<sup>17</sup>, and Rodrigo A. Toledo<sup>1,2</sup>

## ABSTRACT

This study explores parallels between systemic hypoxia adaptation in high-altitude populations and tumorigenesis. We identified *EPAS1*, a gene critical for hypoxia adaptation in populations such as Tibetans and Sherpas, as playing a similar adaptive role in tumors arising under hypoxic conditions. Tumors from patients with chronic hypoxia displayed impaired DNA repair and frequent emergence of *EPAS1* variants, with frequencies reaching up to 90%, echoing the positive selection seen in high-altitude dwellers. Mechanistically, *EPAS1* gain-of-function mutations promote *COX4I2* expression, reducing cellular oxygen consumption and supporting tumor proliferation in hypoxia. Analysis of clinical data from patients with hypoxia revealed tissue-specific and time-sensitive tumorigenic effects, particularly impacting oxygen-sensitive cells in the postnatal period. Our findings suggest that *EPAS1*-driven adaptation mechanisms in high-altitude populations provide a model for understanding tumor evolution under hypoxic stress, highlighting how genetic adaptations to diverse stressors in natural populations may yield insights into tumorigenesis and cancer progression.

**SIGNIFICANCE:** This study reveals a broad convergence in genetic adaptation to hypoxia between natural populations and tumors, suggesting that insights from natural populations could enhance our understanding of cancer biology and identify novel therapeutic targets.

<sup>1</sup>Biomarkers and Clonal Dynamics Group, Vall d'Hebron Institute of Oncology (VHIO), Vall d'Hebron Barcelona Hospital Campus, Barcelona, Spain. <sup>2</sup>Centro de Investigación Biomédica en Red de Cáncer (CIBERONC), Instituto de Salud Carlos III (ISCIII), Madrid, Spain. <sup>3</sup>Department of Medicine, Universitat Autònoma de Barcelona, Bellaterra, Spain. <sup>4</sup>Health Research Institute of Asturias (ISPA), University of Oviedo, Oviedo, Spain. <sup>5</sup>Institute of Oncology of Asturias (IUOPA), University of Oviedo, Oviedo, Spain. <sup>6</sup>Adult Congenital Heart Disease Unit, Department of Cardiology, Hospital Universitario La Paz, Madrid, Spain. <sup>7</sup>Hereditary Endocrine Cancer Group, Human Cancer Genetics Program, Spanish National Cancer Research Centre (CNIO), Madrid, Spain. <sup>8</sup>Oncology Data Science (ODysSey) Group, Vall d'Hebron Institute of Oncology (VHIO), Vall d'Hebron Barcelona Hospital Campus, Barcelona, Spain. <sup>9</sup>Molecular Oncology Group, Vall d'Hebron Institute of Oncology (VHIO), Vall d'Hebron Barcelona Hospital Campus, Barcelona, Spain. <sup>10</sup>Cancer Epigenetics and Nanomedicine Laboratory, Nanomaterials and Nanotechnology Research Center (CINN-CSIC), University of Oviedo, Oviedo, Spain. <sup>11</sup>Department of Organisms and Systems Biology (B.O.S.), University of Oviedo, Oviedo, Spain. <sup>12</sup>Centro de Investigación Biomédica en Red de Enfermedades Raras (CIBERER), Instituto de Salud Carlos III (ISCIII), Madrid, Spain. <sup>13</sup>Integrated Adult Congenital Heart Disease Unit, Department of Cardiology, Vall d'Hebron Hospital Universitario, Vall d'Hebron Barcelona Hospital Campus, Barcelona, Spain. <sup>14</sup>Centro de Investigación Biomédica en Red de Enfermedades Cardiovasculares (CIBERCV), Instituto de Salud Carlos III (ISCIII), Madrid, Spain. <sup>15</sup>European Reference Network for Rare, Low-Prevalence, or Complex Diseases of the Heart (ERN GUARD-Heart), Amsterdam, the Netherlands. <sup>16</sup>Department of Endocrinology and Nutrition, Hospital Universitario La Paz, Madrid, Spain. <sup>17</sup>Division of Hematology and Medical Oncology, Department of Medicine, Mays Cancer Center, University of Texas Health Science Center, San Antonio, Texas. <sup>18</sup>Department of Pathology, University of Texas Health Science Center, San Antonio, Texas. <sup>19</sup>Institute of Clinical Chemistry and Laboratory Medicine, University Hospital Carl Gustav Carus, Medical Faculty Carl Gustav Carus, Technische Universität Dresden, Dresden, Germany. <sup>20</sup>Vall d'Hebron Institute of Oncology (VHIO), Vall d'Hebron Barcelona Hospital Campus, Barcelona, Spain. <sup>21</sup>Department of Pathology, Hospital Universitario La Paz, Madrid, Spain. <sup>22</sup>Department of Pathology, Vall d'Hebron Hospital Universitario, Vall d'Hebron Barcelona Hospital Campus, Universitat Autònoma de Barcelona (UAB), Barcelona, Spain. <sup>23</sup>Cancer Genetics, Kolling Institute, Royal North Shore Hospital, Sydney, Australia. <sup>24</sup>The University of Sydney, Sydney, Australia. <sup>25</sup>Department of Endocrinology, St. Vincent's Hospital, Sydney, Australia. <sup>26</sup>School of Clinical Medicine, Faculty of Medicine and Health, University of New South Wales, Sydney, Australia. <sup>27</sup>Department of Endocrinology and Nutrition, Hospital

Universitario de Basurto, Bilbao, Spain. <sup>28</sup>Department of Pediatric Cardiology, Hospital Universitario Ramón y Cajal, Madrid, Spain. <sup>29</sup>Department of Pediatric Cardiology, Instituto de Investigación Biomédica (Cardiopatía Estructural y Congénita) and Complejo Hospitalario Universitario A Coruña, A Coruña, Spain. <sup>30</sup>Department of Functional Biology, Genetic Area, University of Oviedo, Oviedo, Spain. <sup>31</sup>Endocrinology Division, Hospital das Clínicas, University of São Paulo School of Medicine, São Paulo, Brazil. <sup>32</sup>AP-HP, Hôpital Européen Georges Pompidou, Département de Médecine Génomique des Tumeurs et des Cancers, Paris, France. <sup>33</sup>Inserm, Centre de recherche des Cordeliers, Université Paris-Cité, Sorbonne Université, Equipe Labellisée Ligue Contre le Cancer, Paris, France. <sup>34</sup>Adult Congenital Heart Program, Division of Cardiology, Oregon Health and Science University, Portland, Oregon. <sup>35</sup>Department of Surgery, University of Tennessee Health Science Center, Memphis, Tennessee. <sup>36</sup>Hospital Universitario Central de Asturias, Oviedo, Spain. <sup>37</sup>Adult Congenital Heart Disease Unit, Department of Cardiology, Hospital Universitari i Politècnic La Fe, Valencia, Spain. <sup>38</sup>School of Medicine, University of São Paulo, São Paulo, Brazil. <sup>39</sup>Department of Endocrinology and Cancer Genetics Unit, Kolling Institute, Royal North Shore Hospital, Sydney, Australia. <sup>40</sup>Neuroendocrine and Endocrine Tumor Translational Research Program (NET-VHIO), Vall Hebron Institute of Oncology (VHIO), Vall d'Hebron Barcelona Hospital Campus, Barcelona, Spain. <sup>41</sup>Department of Medical Oncology, Gastrointestinal and Endocrine Tumor Unit, Vall d'Hebron Hospital Universitario, Vall d'Hebron Hospital Campus, Barcelona, Spain. <sup>42</sup>Division of Endocrinology, Mayo Clinic, Rochester, Minnesota. <sup>43</sup>Cincinnati Adult Congenital Heart Disease Program, Heart Institute, Cincinnati Children's Hospital, University of Cincinnati, Cincinnati, Ohio. <sup>44</sup>Department of Cardiology, Boston Children's Hospital, Harvard Medical School, Boston, Massachusetts. <sup>45</sup>Division of Endocrinology, Diabetes, and Hypertension, Department of Medicine, Brigham and Women's Hospital, Harvard Medical School, Boston, Massachusetts. <sup>46</sup>Universitat Pompeu Fabra (UPF), Barcelona, Spain. <sup>47</sup>Department of Endocrinology and Nutrition, Vall d'Hebron Hospital Universitario, Vall d'Hebron Barcelona Hospital Campus, Barcelona, Spain. <sup>48</sup>Department of Neuroimmunology, Center for Brain Research, Medical University of Vienna, Vienna, Austria. <sup>49</sup>Department of Physiology and Pharmacology, Karolinska Institutet Stockholm, Sweden. <sup>50</sup>University of Vic – Central University of Catalonia, Vic, Spain.

**Corresponding Author:** Rodrigo A. Toledo, Biomarkers and Clonal Dynamics Group, Vall d'Hebron Institute of Oncology (VHIO), Vall d'Hebron Barcelona Hospital Campus, Barcelona 08035, Spain; Centro de Investigación Biomédica en Red de Cáncer (CIBERONC), Instituto de Salud Carlos III (ISCIII), Madrid 28029, Spain. E-mail: rtoledo@vhio.net

Cancer Discov 2025;XX:1–26

## INTRODUCTION

Atmospheric oxygen emerged approximately 2.3 billion years ago and triggered essential cellular, developmental, biochemical, and physiological adaptations that were pivotal for survival and evolution of life (1), of which ancestral bacteria (endosymbiotic *Alphaproteobacterium*; ref. 2) integration allowed mitochondrial respiration of molecular oxygen (O<sub>2</sub>) through the electron transport chain (ETC), causing a 15-fold increase in ATP production compared with anaerobic metabolism. Mitochondria also play key roles in biomolecular anabolism and signal transduction via various mechanisms, including reactive oxygen species production (3, 4). Increased energy availability and enhanced cellular communication have facilitated the emergence of multicellular animals, which require additional adaptations to effectively regulate and respond to fluctuating oxygen levels across different body regions (5). In this context, the transcription factor hypoxia-inducible factor 1 (HIF1) is a key oxygen homeostasis regulator and primarily coordinates adaptive responses to fluctuating cellular oxygen levels (6). During hypoxic events, specific prolines within the oxygen-dependent domain of HIF1 $\alpha$  unit stop undergoing hydroxylation by the prolyl hydroxylase enzymes, preventing the recognition of E3 ubiquitin-protein von Hippel-Lindau (VHL) for 26S proteasomal degradation, leading to its stabilization and translocation to the nucleus, where it binds with the stable HIF1 $\beta$  unit (7–10). This protein complex initiates the expression of numerous genes, including those associated with cell proliferation, migration, metabolic reprogramming (e.g., the Warburg effect and lipid metabolism), and neoangiogenesis, among other processes aimed at restoring oxygen homeostasis of the affected cells.

Throughout evolution, HIF2 $\alpha$ , encoded by the *EPAS1* gene, emerged from HIF1 $\alpha$  by gene duplication. HIF2 $\alpha$  plays a versatile role in regulating adaptations to whole-body (systemic) hypoxia (11–13). Specifically, HIF2 $\alpha$  is required for embryonic development and organ function involved in O<sub>2</sub> sensing and for response to systemic hypoxia, such as the parasympathetic carotid body, sympathetic paraganglia, and adrenal medulla (14). When mature, about a week after birth, these organs function as follows: first, glomus cells within the carotid body sense low O<sub>2</sub> tension in the blood (hypoxemia); second, through afferent splanchnic nerves, the carotid body signals the sympathetic chromaffin cells of the adrenal medulla, which abundantly secrete adrenaline and noradrenaline (collectively known as catecholamines); and third, the nervous stimulus combined with high adrenaline levels elicit a rapid compensatory response to hypoxia, involving hyperventilation, tachycardia, and increased venous tonus (15, 16). Nevertheless, the immature adrenal medulla from birth until day 7 of life, before it gets innervated by the splanchnic nerves, can autonomously detect low oxygen levels and secrete extremely high levels of catecholamines such as norepinephrine into the bloodstream in response to hypoxia, which is crucial for neonatal adaptation to extrauterine life (17, 18).

doi: 10.1158/2159-8290.CD-24-0943

This open access article is distributed under the Creative Commons Attribution-NonCommercial-NoDerivatives 4.0 International (CC BY-NC-ND 4.0) license.

©2025 The Authors; Published by the American Association for Cancer Research

Moreover, HIF2 $\alpha$  is directly involved in adaptation to prolonged hypoxia. For example, when mountaineers climb high-altitude peaks and experience hypobaric hypoxia, HIF2 $\alpha$  is activated in the kidneys and augments erythropoietin (EPO) production, a hormone that stimulates erythropoiesis to enhance oxygen transport and tissue oxygenation (19–21).

Consistent with *EPAS1* evolutionary specialization in systemic hypoxia adaptation, several studies have observed extreme positive selection of *EPAS1* genetic variants in highlanders compared with lowlanders across many species (22–30). *EPAS1* is indicated as a major target of genetic adaptation to high-altitude hypoxia. These highly advantageous *EPAS1* haplotypes in humans and other mammals present a loss-of-function effect in the HIF2 $\alpha$ –EPO axis, avoiding excessive production of red blood cells in hypoxia and augmenting blood perfusion to the organs and periphery (31–34). Beneficial *EPAS1* variants frequently originate from genetic introgression because of reproduction with a related species that is already adapted to hypoxic environments rather than occurring *de novo* (35, 36). For humans, the *EPAS1* haplotype likely originated via archaic introgression from the Denisovans who lived near the Tibetan plateau (36–38) and is currently present in 90% of the highlander Tibetans and Sherpas. This Denisovan-like *EPAS1* haplotype is not found elsewhere, representing the strongest selection of any gene reported in humans (25, 36, 38).

*EPAS1* has also been identified as a *bona fide* oncogene, promoting tumorigenesis and tumor development (39–41). The tumorigenic role of HIF2 $\alpha$  was recently confirmed by the successful use of an on-target HIF2 $\alpha$  inhibitor in hypoxia-driven tumors (42–46). The oncogenic function of *EPAS1* is tissue dependent and impacts cell lineages, wherein it controls embryonic development, such as the carotid body (derived from parasympathetic tissue) and sympathetic paraganglia and adrenal medulla (14). Tumors that arise from these cells sensitive to *EPAS1* are classified as pheochromocytomas or paragangliomas, collectively referred to as PPGL (40, 47, 48). They are challenging for oncological management and characterized by rarity, therapeutic orphan status, the absence of biomarkers for metastatic behavior, and a lack of suitable animal models. PPGLs are highly heritable neoplasms frequently driven by single, mutually exclusive germline or somatic mutations, which often directly or indirectly activate HIF2 $\alpha$  (49, 50). Earlier studies suggested that environmental systemic hypoxia, resulting from high-altitude environments in the Andes and Colorado (51–53), or pathological cyanotic congenital heart disease (CCHD), could pose a risk for PPGL development (54). Epidemiological studies have estimated that patients with CCHD have a sixfold higher chance of developing PPGL than the general population or individuals with non-CCHD (54, 55).

The combination of systemic hypoxia, usually since birth, and increased risk of developing PPGL makes patients with CCHD unique human models for studying the role of hypoxia in tumorigenesis. Recent studies, including those from our group, have revealed that PPGLs from patients with systemic hypoxia, such as CCHD or sickle cell disease, harbor somatic gain-of-function mutations in the *EPAS1* gene (56–59); however, their mechanistic consequences remain largely unknown.

In this study, we explored genetic, *in vitro*, population and clinical data to determine the mechanism, time of occurrence, and reason for *EPAS1* mutation generation in tumors developed under systemic hypoxia. We identified significant molecular convergence between human tumors from patients with chronic systemic hypoxia and humans adapted to high-altitude hypoxia, such as Tibetans and Sherpas. Our study reveals a previously unrecognized level of convergence in which natural populations and tumor cells subjected to similar environmental stressors, such as hypoxia, develop analogous genetic and molecular adaptations. This discovery could guide future studies on the links between natural adaptation and tumorigenesis, paving the way for the identification of new tumor drivers and therapeutic vulnerabilities.

## RESULTS

### Highly Frequent *EPAS1* Clonal Mutations in Sympathetic PPGL Tumors Developed under Systemic Hypoxia

We assembled and examined a large cohort of 34 PPGL tumor samples collected from 27 patients with CCHD across five distinct countries (Supplementary Figs. S1 and S2; Supplementary Table S1). We investigated the *EPAS1* status, potential genotype–phenotype correlations, and underlying molecular mechanisms of tumor adaptation and survival under systemic hypoxia. Most tumors (27/34, 79.4%) were sympathetic catecholamine-secreting PPGLs, comprising pheochromocytomas and/or thoracic and abdominal paragangliomas. Targeted Sanger sequencing revealed *EPAS1* mutations in 24/27 sympathetic CCHD-PPGLs (88.8%). All mutations occurred exclusively in the tumor DNA and not in the germline DNA, clustered within the oxygen-dependent degradation domain of HIF2 $\alpha$  (60), being all missense alterations (L529P, A530P/T/V, P531A/R/L/S, Y532C, and L542R/P) except one in-frame deletion (P534\_N536del; Supplementary Table S1). A total of 12/14 (85.7%) thoracic and abdominal paragangliomas and 12/13 (92.3%) pheochromocytomas were mutated (Fig. 1A). Two patients with multiple tumors carried a distinct *EPAS1* missense somatic mutation (P16 and P21; Fig. 1B). Whole-exome sequencing (WES) excluded germline or somatic mutations in other known PPGL susceptibility genes, emphasizing the significance of *EPAS1* mutations as CCHD-PPGL tumor genetic driver. These results highlight a strong convergent evolution of *EPAS1* in PPGL tumorigenesis under systemic hypoxia at the inter- and intrapatient levels.

Only 8/178 (4.5%) PPGLs from patients from The Cancer Genome Atlas (TCGA) project, without CCHD (61), carried an *EPAS1* mutation, indicating a 20-fold increase in *EPAS1* mutation frequency in patients with hypoxia vs. normoxia (88.8% vs. 4.5%;  $P < 0.0001$ ; Fig. 1A). Selection inference confirmed that *EPAS1* was the only gene under statistically significant and strong positive selection in our CCHD-PPGL cohort, with  $dN/dS = 702$  ( $q = 0$ ; Supplementary Table S2). When further stratifying by tissue type, the inferred selection strength increases to  $dN/dS = 926$  in the sympathetic subcohort, whereas  $dN/dS = 0$  in the parasymphetic subcohort, as all *EPAS1* mutations were found in sympathetic PPGLs. In PPGL tumors from patients without CCHD of the TCGA,

*EPAS1* was the gene with the third largest signal of positive selection (after *HRAS* and *NFI*) and marginally significant ( $dN/dS = 110$ ;  $q = 0.1$ ; Supplementary Table S2). This contrasts with the rest of the TCGA cohort, in which *EPAS1* is not selected, neither at the pan-cancer level nor in any of the individual cancer types.

Furthermore, we assessed the neoplastic cell proportion of *EPAS1*-mutated (*EPAS1*<sup>MUT</sup>) clones in PPGL tumors developed in normoxia (TCGA cohort) and in systemic hypoxia (CCHD cohort) via calculating the cancer cell fraction (CCF; ref. 62). *EPAS1* mutations presented extremely high CCF levels in both cohorts (median of 1 and 0.99), a result that clearly supports *EPAS1* mutations as the initial genetic events in PPGLs (Fig. 1C; Supplementary Figs. S3 and S4; Supplementary Tables S3–S5).

### *EPAS1* Mutation Absence in Parasympathetic PPGL Tumors and across Tumor Types

Contrasting the extreme high and moderate *EPAS1* mutation frequency in sympathetic PPGL tumors from patients with CCHD (24/27, 88.8%) and in sympathetic PPGL tumors from patients without CCHD (TCGA; 8/178, 4.5%), respectively, targeted sequencing identified no *EPAS1* mutations in seven parasymphetic carotid body PPGLs from patients with CCHD (0/7; Supplementary Fig. S5). WES of four of these tumors showed no mutations in complete coding regions of the *EPAS1* gene, its homolog genes *HIF1A* and *HIF3A*, and any known PPGL-related pseudohypoxia genes. No *EPAS1* mutations were detected in additional parasymphetic PPGLs from patients without CCHD: 0/52 from a previous cohort (63) and 0/214 from an unpublished cohort that we collected (see the Methods section of ref. 64;  $P < 0.00001$ ; Supplementary Fig. S5). Furthermore, *EPAS1* mutations were extremely rare across 33 human cancer types from the 212 studies available on cBioPortal (5/69,045 tumor samples, 0.007%; ref. 65) and TCGA Pancancer Atlas Studies (0/10,775 tumor samples, 0%; Supplementary Tables S1 and S6; ref. 66). These results suggest that *EPAS1* somatic mutations occur exclusively in PPGL tumors of sympathoadrenal lineage and are 20-fold enriched in CCHD (systemic hypoxia; Fig. 1D; Supplementary Fig. S6A–S6C).

### *EPAS1* Evolutionary Trajectory in Systemic Hypoxia-Developed PPGL Tumors Parallels That Observed in Highlander Tibetans and Sherpas

*EPAS1* genetic variants are rarely observed from numerous samples sequenced from global populations living at low altitudes or from tumor samples across more than 30 tumor types. By contrast, we detected *EPAS1* mutations in 89% sympathetic PPGL tumors in patients with CCHD, paralleling the 90% *EPAS1* variant prevalence reported in Tibetans and Sherpas in the Himalayas (Fig. 1D; refs. 23, 25, 36, 37). This level of extreme positive selection and genetic variant fixation is rare in natural populations. For Tibetans, *EPAS1* variants were likely introgressed by archaic Denisovans to early modern human populations (36), probably when both species co-inhabited the Tibetan plateau 30 to 45 thousand years ago (67–69). Introgression and selection sweep of advantageous *EPAS1* genetic variants have been reported in different

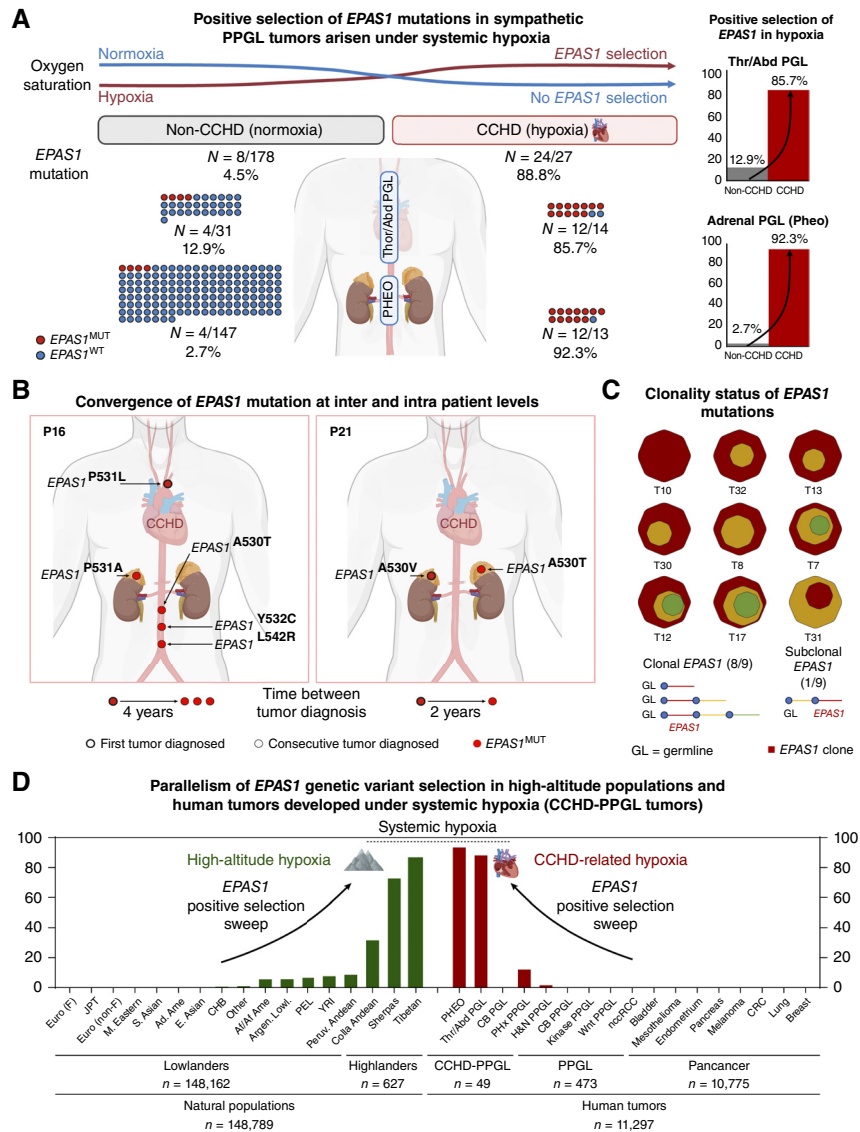


**Figure 1.** Convergent positive selection of *EPAS1* genetic variant in hypoxia-developed PPGL tumors and high-altitude populations. **A**, Positive selection of *EPAS1* mutations in our cohort of PPGL tumors from patients born with CCHD and systemic hypoxia (24/27, 88.8%, right side) compared with those without (non-CCHD cohort from the TCGA, 8/178, 4.5%, left side). Red circle: *EPAS1*<sup>MUT</sup> (*EPAS1*-mutated); blue circle: *EPAS1*<sup>WT</sup> (*EPAS1*-WT). Considering tumor location, *EPAS1* mutations were highly enriched in thoracic and abdominal paraganglioma (PGL) from patients with CCHD compared with non-CCHD (85.7% vs. 12.9%) and in pheochromocytomas (Pheo) from patients with CCHD compared with non-CCHD (92.3% vs. 2.7%). **B**, *EPAS1* mutational convergence in patients with multiple primary CCHD-PPGLs. Patient 16 (left) developed five independent primary tumors. The first PGL tumor was diagnosed in the mediastinum of the patient at 29 years of age; 4 years later, the patient developed three periaortic paragangliomas and a right pheochromocytoma, each carrying a different *EPAS1* missense mutation (A530T, P531A, P531L, Y532C, and L542R). Patient 21 (right) developed metachronous bilateral pheochromocytoma (the first at 32 years of age) within a 2-year period, and each tumor carried a different *EPAS1* mutation (named A530V and A530T). Patient 1 (not shown) presented with an *EPAS1*<sup>WT</sup> carotid body and 2 months later was diagnosed with a left pheochromocytoma that harbored an *EPAS1* mutation (P531S). Bold outline circle: first tumor diagnosed; black outline circle: consecutive tumors diagnosed; red circle: *EPAS1*<sup>MUT</sup>. **C**, Clonality analysis of *EPAS1* mutations in CCHD-PPGL tumors: 8/9 (88%) tumors harbored an *EPAS1* clonal mutation with a median CCF of 0.99, Supplementary Figs. S3 and S4; Supplementary Tables S3–S5. The clone in which *EPAS1* mutation is included is represented in red. **D**, Allele frequencies of *EPAS1* genetic variants for different populations living in high- and low-altitude regions (left side, in green) and for different tumor type cohorts from patients with normoxia from publicly available cancer genomics databases and for PPGL tumors from patients with CCHD developed under hypoxia (right side, in red color). The figure displays a representation of the entire cohort of individuals and tumor samples analyzed, listed in Supplementary Table S6. Functional *EPAS1* genetic variants are extremely positively selected exclusively in natural populations that are genetically adapted to high-altitude hypoxia (up to 87% in Tibetans) and in sympathetic PPGL tumors from patients with CCHD born with hypoxia (up to 90%). By contrast, *EPAS1* variants are extremely rare and mostly absent in all lowlander populations and in cancer cohorts from patients with normoxia; non-CCHD sympathetic PPGLs harboring up to 4.5% of *EPAS1* mutations were the exception. These results strongly support systemic hypoxia as a major driver of *EPAS1* genetic variant-positive selection in natural populations and in human tumors (see Supplementary Table S6). Ad. Ame, admixed American; Af/Af Ame, African/American; Argen. Lowl., Argentinian lowlanders; CB, carotid body; CHB, Han Chinese in Beijing; CRC, colorectal cancer; E. Asian, East Asian; Euro (F), European (Finnish); Euro (non-F), European (non-Finnish); H&N, head and neck; JPT, Japanese in Tokyo; M. Eastern, Middle Eastern; nccRCC, non-clear-cell renal cell carcinomas; PEL, Peruvians residing in Lima; Peruv. Andean, Quechua Peruvian Andean highlanders; Phx, pseudohypoxia; PPGL, pheochromocytomas and paragangliomas; S. Asian, South Asian; Thr/Abd, thoracic/abdominal; YRI, Yoruba from Ibadan. (**A** and **B**, Created with BioRender.com.)

Downloaded from <http://aacrjournals.org/cancerdiscovery/article-pdf/doi/10.1158/2159-8290.CD-24-0943> by guest on 10 April 2025

species and animal populations living at high altitudes (Fig. 1D; Supplementary Fig. S7A–S7E; Supplementary Table S6; refs. 26–30) and represent the most common and efficient hypoxia adaptation method. The positive selection of introgressed *EPAS1* genetic variants in Himalayan populations indicates that evolutionary introgression is an accelerated evolution mechanism that greatly facilitates hypoxia adaptation (Supplementary Fig. S8). Other human populations living at similar altitudes as the Tibetans, such as Colla Andean from Argentina and Peruvian Andean (living in altitudes up to 4,450 m), present marked maladaptation features, that is, high-altitude or chronic mountain sickness (70, 71). The high Andes was inhabited more recently than the Tibet plateau (approximately 10 thousand vs. 40 thousand years ago) and without indicating genetic introgression (72–75). Therefore, both the Peruvian Andean and Colla Andean populations harbor lower *EPAS1* genetic variants than the Tibetans (9% vs. 32% vs. 90%, respectively, Fig. 1D; Supplementary Tables S6 and S7; refs. 72–75).

The evolutionary parallelism observed in high-altitude dwellers and in PPGL tumors from patients with CCHD who experience systemic hypoxia since birth is unique. In natural populations, this phenomenon is propelled by accelerated adaptation and characterized by introgression and selection sweeps (36, 38, 68, 76). Likewise, we identified and characterized that CCHD-PPGL tumors developed under systemic hypoxia likely harbored an accelerated process that enhanced hypoxia adaptation, as follows.

### Faulty DNA Repair and Increased Mutation Burden in Systemic Hypoxia-Developed Tumors

Previous studies showed decreased DNA repair, increased mutability, and increased adaptability in tumor cell lines cultivated under hypoxic stress (77–83) and increased tumor mutational burden (TMB) in tumors with increased intratumoral hypoxia, measured by RNA sequencing (RNA-seq)-based signatures (77, 78); hence, we hypothesized that similar processes could be driven by systemic hypoxia. Our results showed that non-neoplastic tissues adjacent to tumors stained positive for microsatellite instability (MSI) proteins, which was expected; however, most *EPAS1*<sup>MUT</sup> sympathetic PPGL tumors from patients with hypoxic CCHD displayed faulty DNA repair system proteins (Supplementary Fig. S9). Specifically, 7/9 (77%) tumors available for IHC staining presented evidence of MSI, characterized by the expression loss of mismatch repair proteins, such as MLH1, MSH2, MSH6, and PMS2 (Fig. 2A), which indicated reduced DNA repair function. On the contrary, all four *EPAS1* wild type (*EPAS1*<sup>WT</sup>) parasympathetic CCHD-PPGL tumors expressed MSI marker proteins MLH1, PMS2, MSH2, and MSH6 (Fig. 2B). Differences in MSI statuses between tumors from the sympathetic and parasympathetic lineages are clear, 77% versus 0%, and semi-quantitative H-score quantification as shown in Fig. 2C. MSI generally occurs in 3% to 4% of human tumors (exception being colorectal tumors with 20% MSI; ref. 84). Therefore, the link between systemic hypoxia and MSI status that we found in sympathetic CCHD-PPGLs is noteworthy. We generated WES data of nine sympathetic CCHD-PPGL tumors developed under hypoxia from our cohort and compared them

with sympathetic PPGL tumor samples from patients without CCHD from the TCGA cohort (61) and Calsina and colleagues (85). We observed a significantly higher average MSI genomic score, global copy number (CN) alterations, and tumor mutation in the sympathetic CCHD-PPGL tumors developed under hypoxia (average of 15 somatic mutations vs. 9 somatic mutations;  $P = 0.02$ ; Fig. 2D–F; Supplementary Table S8). These results suggest a process of accelerated adaptability within sympathetic CCHD-PPGL tumors developed under hypoxia via hampering DNA repair and increasing the genetic instability and mutation pool within the tumor, which may favor the occurrence of *EPAS1* mutations that are then strongly selected during hypoxia (Supplementary Fig. S10).

### Prolonged Hypoxia Leads to Increased DNA Damage in PPGL-Derived PC12 Cells

We further investigated the relationship between hypoxia and DNA damage *in vitro* by assessing the levels of  $\gamma$ H2AX, a phosphorylated form of H2AX widely recognized as a marker of DNA damage, and PARP1, which plays a key role in stabilizing DNA replication forks. Using immunofluorescence and Western blot analyses, we observed low levels of  $\gamma$ H2AX in PC12 PPGL tumor-derived cells cultured under normoxic conditions (21% O<sub>2</sub>), maintained across both short-term and long-term cultures (up to 36 days), suggesting minimal DNA damage induction in normoxia. By contrast, cells exposed to hypoxic conditions (1% O<sub>2</sub>) exhibited an activation of  $\gamma$ H2AX, with a significant increase in  $\gamma$ H2AX levels after prolonged hypoxia (1% O<sub>2</sub> for 36 days). Conversely, PARP1 levels progressively declined under hypoxia, with a pronounced reduction observed after prolonged hypoxic exposure (1% O<sub>2</sub> for 36 days), as shown in Fig. 3A and B; Supplementary Fig. S11A–S11D. These findings were corroborated by comet assay results, which demonstrated substantial DNA damage in PC12 cells subjected to long-term hypoxia compared with those maintained in normoxia (Fig. 3C). Collectively, these data imply that sustained hypoxic conditions induce DNA damage in PC12 cells, as evidenced by increased  $\gamma$ H2AX and comet assay findings, and concurrently diminishing PARP1 levels, potentially compromising DNA repair capacity.

### Elevated Fumarate and Reduced Succinate Levels in *EPAS1*-Mutated PPGL Tumors and a PPGL Cellular Model

Mitochondrial oncometabolites, including succinate and fumarate, are known to disrupt DNA repair mechanisms by inhibiting  $\alpha$ -ketoglutarate-dependent dioxygenases, such as lysine demethylases (86). In this study, we analyzed these metabolites across a cohort of human PPGL tumors ( $N = 141$ ; ref. 148) with varying genotypes, including *EPAS1*-mutated, *VHL*-mutated, and *SDHx*-mutated (*SDHA*, *SDHB*, *SDHC*, *SDHD*, and *SDHAF2*) pseudohypoxic tumors. Our results showed that *EPAS1*-mutated (and *VHL*-mutated) tumors exhibited significantly elevated fumarate levels alongside reduced succinate levels (Fig. 3D; Supplementary Fig. S12), and such a metabolic profile was associated with the expression levels

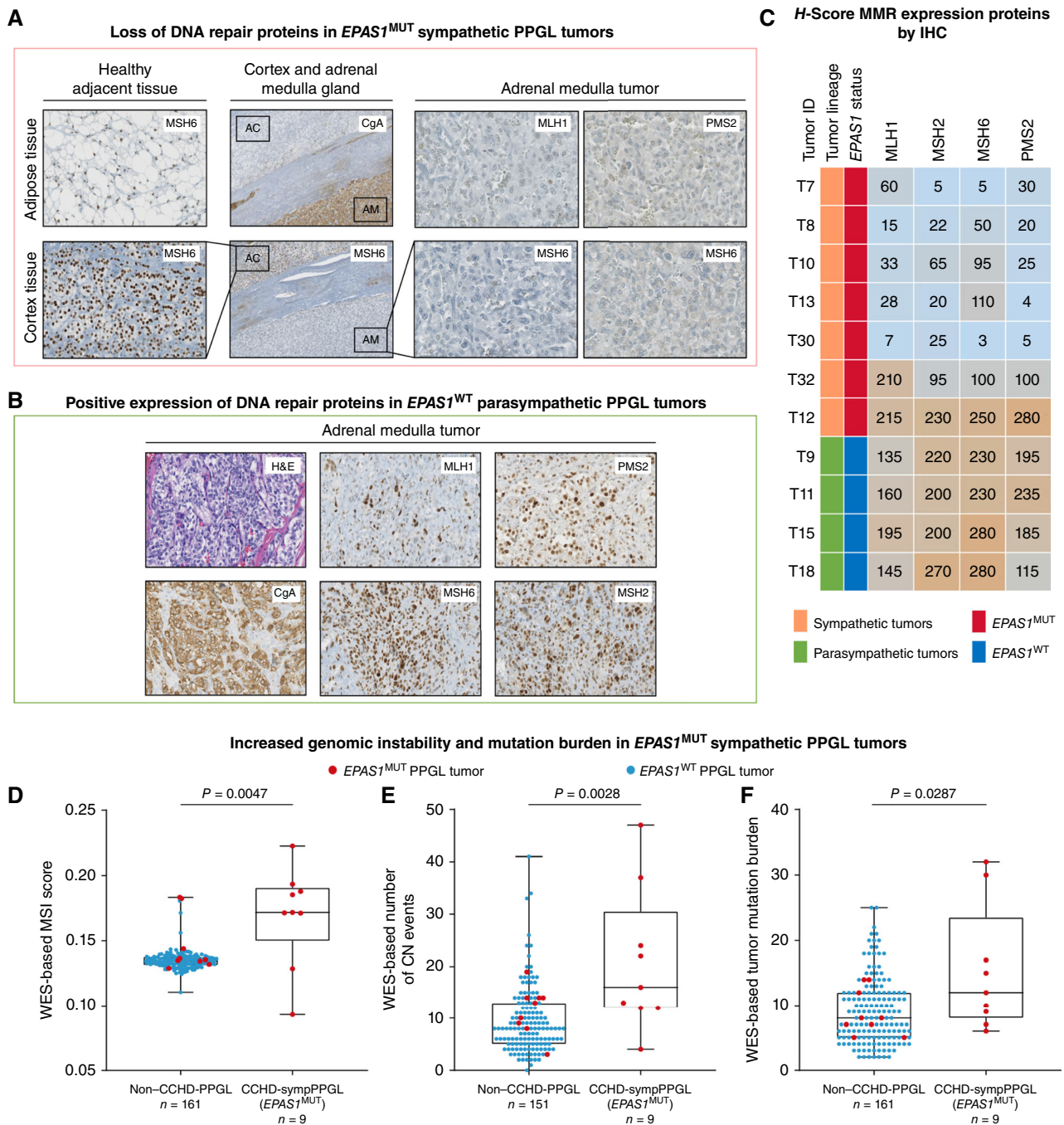


**Figure 2.** Impaired DNA repair and increased mutation burden in systemic hypoxia-developed tumors. **A**, IHC staining showing decreased expression of DNA repair machinery proteins observed in most *EPAS1*<sup>MUT</sup> sympathetic PPGL tumors from patients with CCHD (7/9, 77.7%). Results of *EPAS1*<sup>MUT</sup> sympathetic PPGL tumor T7 are shown: (i) expected positive expression of the MSH6 MSI biomarker in PPGL tumor-surrounding tissues from patients with CCHD, such as adipose and adrenal cortical (40× magnification); (ii) positive expression of chromogranin A in the adrenal medulla (PPGL tumor) and not cortex; (iii) positive expression of MSH6 in the adrenal cortex but not in the PPGL tumor (10× magnification), and (iv) decreased expression of MSI biomarkers such as MLH1, MSH2, MSH6, and PMS2 in the CCHD-PPGL neoplastic cells (40× magnification). **B**, When compared with PPGL parasymphatic tumor with *EPAS1*<sup>WT</sup> status (T18), all MSI biomarkers show a positive expression in the non-neoplastic and neoplastic cells. Hematoxylin and eosin and chromogranin A are also indicated as positive controls. **C**, IHC from MSI biomarkers in available tumor samples, scored semiquantitatively using an H-score for the nucleus. PPGL sympathetic tumors have a diminished H-score (<100; 6/7, 86%), whereas all parasymphatic tumors present higher H-scores, indicating differences of mismatch repair protein (MMR) expression between tumor lineages. Detailed IHC images are shown in Supplementary Fig. S9, which include seven sympathetic PPGL tumors. A total of nine sympathetic PPGL tumor samples were analyzed; in two of them, only the PMS2 marker was assessed due to limited sample availability (T3: H-score = 1, T4: H-score = 75), and their images are not shown. **D-F**, Germline-tumor-paired WES data were used to compare MSI score, CN alterations burden (number of CN events), and TMB between sympathetic PPGL (sympPPGL) tumors from patients without and with CCHD (N = 161, left, and N = 9, right, respectively; refs. 61, 85). *P* values calculated using Mann-Whitney *U* test. Red circle: *EPAS1*<sup>MUT</sup> tumors and blue circle: *EPAS1*<sup>WT</sup>. CN, copy number; H&E, hematoxylin and eosin; IHC, immunohistochemistry; MMR, mismatch repair; MSI, microsatellite instability; WES, whole-exome sequencing.

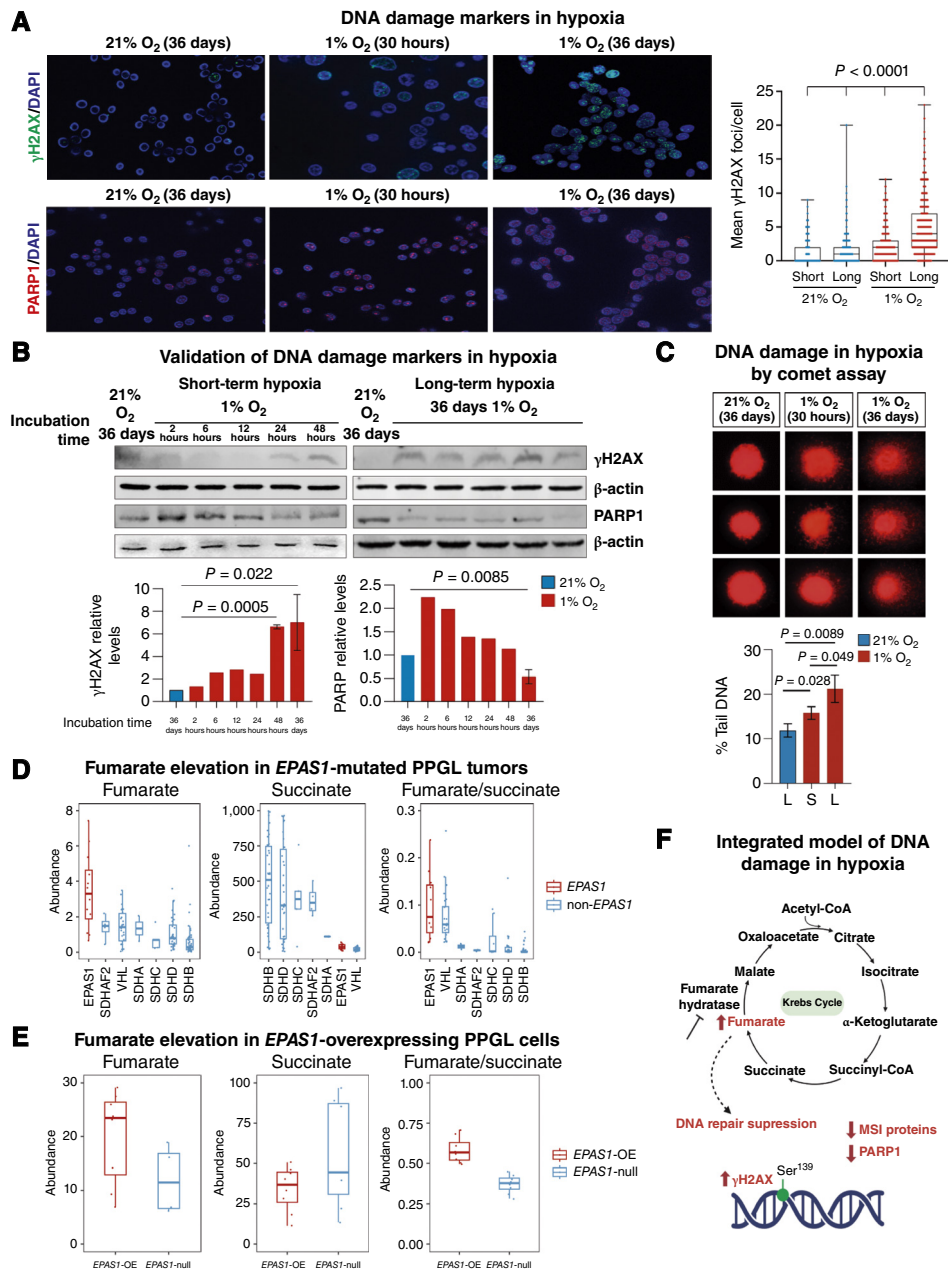


**Figure 3.** Measurements of hypoxia-driven DNA damage and DNA damaging metabolites in PC12 PPGL tumor-derived cells, *EPAS1*-mutated PPGL tumors and *EPAS1*-overexpressing pheochromocytoma-derived cells (*EPAS1*-OE). **A**, Representative immunofluorescence images showing  $\gamma$ H2AX foci formation and PARP1 expression in PC12 cells exposed to hypoxia (1% O<sub>2</sub>) for 30 hours (short hypoxia) or 36 days (long hypoxia), or maintained under normoxic (21% O<sub>2</sub>) conditions (left); quantification of the mean  $\gamma$ H2AX foci per cell (right). **B**, Representative immunoblot images (above) and quantification of the indicated proteins (below) in PC12 cells exposed to normoxia or hypoxia for the specified timepoints. **C**, Comet assay analysis of DNA damage in PC12 cells exposed to normoxia (21% O<sub>2</sub>) for 36 days or hypoxia (1% O<sub>2</sub>) for 30 hours or 36 days (above); representative immunofluorescence images of comet tails:tail moment quantification. About 50–100 cells were scored per condition in each independent experiment (below). A higher percentage of DNA in the tail correlates with increased DNA damage. PC12 cells exposed to hypoxia for 30 hours exhibited significantly higher levels of DNA damage than cells cultured under normoxic conditions (15.75% vs. 11.80% tail DNA;  $P = 0.028$ ). In addition, prolonged hypoxic exposure (up to 36 days) led to an even greater percentage of DNA in the comet tail (21.22% vs. 11.80% tail DNA;  $P = 0.0089$ ), suggesting a deficiency in DNA repair mechanisms under these conditions. L, long; S, short. **D**, Elevated levels of fumarate metabolite in *EPAS1*-mutated PPGL tumors and increased levels of succinate metabolite in *SDHx*-mutated pseudohypoxic PPGL tumors. Metabolite analyses of fumarate, succinate, and fumarate/succinate ratio in *EPAS1*-mutated PPGL tumors ( $n = 12$ , red) and *VHL*- and *SDHx*-mutated pseudohypoxic PPGL tumors (*EPAS1*-WT tumors,  $n = 129$ , blue) as already described (148).  $P$  values of the statistical significance between *EPAS1*-mutated tumors vs *EPAS1*-WT tumors were calculated using the Wilcoxon test. Supplementary Figure S12 shows the results of all  $P$  values calculated using the Wilcoxon test; only significant  $P$  values are indicated. **E**, Increased levels of fumarate/succinate metabolite in *EPAS1*-OE cells. Metabolite analyses of fumarate, succinate, and fumarate/succinate ratio in MPCmCherry cells transfected with an overexpressing *EPAS1*-HIF2 $\alpha$  (*EPAS1*-OE,  $n = 8$ , red) and empty vector as control (*EPAS1*-null, empty vector,  $n = 8$ , blue) as described by Bechmann and colleagues (87). Supplementary Figure S15 shows the  $P$  values calculated using the Wilcoxon test. **F**, Model of DNA damage and oncometabolites implication in *EPAS1*-mutated tumor PPGLs and PPGL cell models with *EPAS1* mutation or cultured under long-term hypoxia conditions. OE, overexpression. (**F**, Created with BioRender.com.)

of genes encoding key enzymes involved in the conversion of succinate to fumarate (*SDHB*, succinate dehydrogenase) and fumarate to malate (*FH*, fumarate hydratase, also known as fumarase; Supplementary Figs. S13A–S13D and S14).

To further validate these findings, we performed metabolomic profiling on a mouse model of pheochromocytoma (MPC) cells with and without HIF2 $\alpha$  overexpression (87). The metabolic profile of MPC cells overexpressing HIF2 $\alpha$  closely resembled that of *EPAS1*-mutated tumors, with increased fumarate, decreased succinate levels, and increased fumarate/succinate levels (Fig. 3E; Supplementary Fig. S15). Collectively, our data, derived from both human *EPAS1*-activated PPGL tumors and a PPGL cellular model, consistently indicate a disruption of oncometabolites that correlate with impaired DNA repair processes (Fig. 3F).

### Mitochondrial Respiration Modulation As a Potential Mechanism for Hypoxia Adaptation Driven by *EPAS1* Mutations in Systemic Hypoxia Tumors

We investigated the molecular foundation underlying the extreme *EPAS1* mutation selection in sympathetic CCHD-PPGL tumors developed under hypoxia. Previous studies from our group and others showed that *EPAS1* missense genetic variants in PPGLs were gain-of-function mutations and promoted tumor formation *in vivo* via hampering VHL-dependent proteasomal HIF2 $\alpha$  degradation (40, 48). To identify *EPAS1*-HIF2 $\alpha$  target genes involved in systemic hypoxia adaptation among numerous genes transcriptionally controlled by HIF2 $\alpha$ , we compared the data from bulk RNA-seq-based transcription profiles of *EPAS1*<sup>WT</sup> ( $n = 46$ ) and *EPAS1*<sup>MUT</sup> ( $n = 8$ ) PPGL tumors from the TCGA cohort (61) and *EPAS1*<sup>WT</sup> ( $n = 11$ ) and *EPAS1*<sup>MUT</sup> PPGL tumors ( $n = 19$ ) from a cohort with hemoglobin disorders and putative chronic systemic hypoxia (59). Also, new transcription data profiles of the PC12 rat-PPGL-derived cell line cultured at different timepoints (12, 24, and 48 hours and 36 days) under normoxic ( $n = 12$ ) and hypoxic ( $n = 12$ ) conditions (1% O<sub>2</sub>) were included in the analyses (Fig. 4A; Supplementary Tables S9–S11).

From these three cohorts, we found significant overexpression of two genes that encoded mitochondrial proteins: *HMGL1*, involved in leucine and fatty acid metabolism (88), and *COX4I2* (Fig. 4A and B). *COX4I2* warranted further evaluation as cytochrome c oxidase 4 (*COX4*) enzymes are final components of mitochondrial ETC that directly transferred electrons to oxygen and produced important cellular signaling intermediates, such as NADH, reactive oxygen species, water, and ATP (89). Fukuda and colleagues (90) showed that cells cultivated under hypoxia switched expression of ubiquitous *COX4I1* to the atypical *COX4I2* unit, which has a lower oxygen affinity, thus altering mitochondrial respiration under low oxygen conditions (Supplementary Fig. S16). We evaluated *EPAS1* mutation modulation of cellular aerobic respiration. Using the Seahorse respiratory assay, we found that HEK293 cell line that stably expressed *EPAS1* gain-of-function mutation (HIF2 $\alpha$  P405A/P531A) and induced *COX4I2* expression displayed reduced oxygen consumption rate compared with their *EPAS1*<sup>WT</sup>-expressing (HIF2 $\alpha$  WT) counterparts [average 0.73 pmol/minutes/AU (range 0.63–0.87) vs. average 0.83 pmol/minutes/AU (range 0.74–0.92), respectively

( $P < 0.0001$ )] and at basal respiration, an average 0.80 pmol/minutes/AU (range 0.69–0.91) in HIF2 $\alpha$  P405A/P531A and 0.91 pmol/minutes/AU (range 0.81–0.99) in HIF2 $\alpha$  WT ( $P < 0.0001$ ), as shown in Fig. 4C. These results indicate mitochondrial respiration modulation and cellular oxygen consumption optimization via *COX4I2* regulation as the functional molecular mechanism for strong positive *EPAS1* mutation selection in PPGLs generated under low-oxygen conditions.

### Temporal Trajectory of *EPAS1* and *COX4I2* during Embryonic Development and in *EPAS1*-Mutated PPGL Tumors

PPGLs are neural crest-derived tumors (50). To evaluate the link between *EPAS1* and *COX4I2* and its temporal expression dynamics, we analyzed single-cell RNA-seq (scRNA-seq) data comprising the entire neural crest lineage development tree, which included a differentiation trajectory from the neural crest toward chromaffin cells via Schwann cell precursor and Bridge state intermediates (Fig. 4D; ref. 91). We found that *EPAS1* and *COX4I2* expressions were correlated in an immature pre-birth chromaffin cell population, suggesting a common regulatory link that coordinated *EPAS1* and *COX4I2* in similar cells within the same time window in oxygen-sensitive and responsive neural crest-derived cell types (Fig. 4D). These scRNA-seq data highlight key roles of *EPAS1* and *COX4I2* in developing sympathetic systems; they are consistent with the mid-gestational lethality of *EPAS1* knockout mice caused by reduced catecholamine levels causing impaired cardiac function and mitochondrial homeostasis (14, 92). The concordance between scRNA-seq and genetic manipulation underscores the importance of *EPAS1* and *COX4I2* in orchestrating essential processes in immature chromaffin cells for proper sympathetic system development.

Our scRNA-seq data from postnatal chromaffin/adrenal medulla cells after the onset of breathing showed that *EPAS1* and *COX4I2* expressions were downregulated at this later timepoint (Fig. 4D). This suggests a crucial developmental time window for *EPAS1* and *COX4I2*, which is weakened in mature chromaffin/adrenal medulla cells. We observed that *EPAS1*<sup>MUT</sup> PPGL tumors showed a significant resurgence in *EPAS1* and *COX4I2* gene expression, suggesting a fetal-like transcriptional pattern in tumor chromaffin cells (Fig. 4B and D). *EPAS1* and *COX4I2* hyperexpression was confirmed in independent *EPAS1*<sup>MUT</sup> PPGL tumor cohorts (59, 93) and was not observed in *EPAS1*<sup>WT</sup> PPGL tumors, suggesting that it was driven by *EPAS1* mutation-dependent HIF2 $\alpha$  activation (Fig. 4B).

Integrating genetic, scRNA-seq, and bulk RNA data helped delineate a temporal window during embryological development, wherein *EPAS1* and *COX4I2* exhibited coordinated expression in immature chromaffin cells. This coordination diminishes postnatally upon cell maturation but resurfaces during *EPAS1* mutation-driven tumorigenesis.

### Temporal and Tissue-Specific Impact of Systemic Hypoxia in Tumorigenesis

Through the CCHD-PPGL International Consortium, we built and curated a large dataset comprising 2,588 patients, including 1,599 patients diagnosed with CCHD without PPGL; 840 patients with PPGL without CCHD (tumors developed

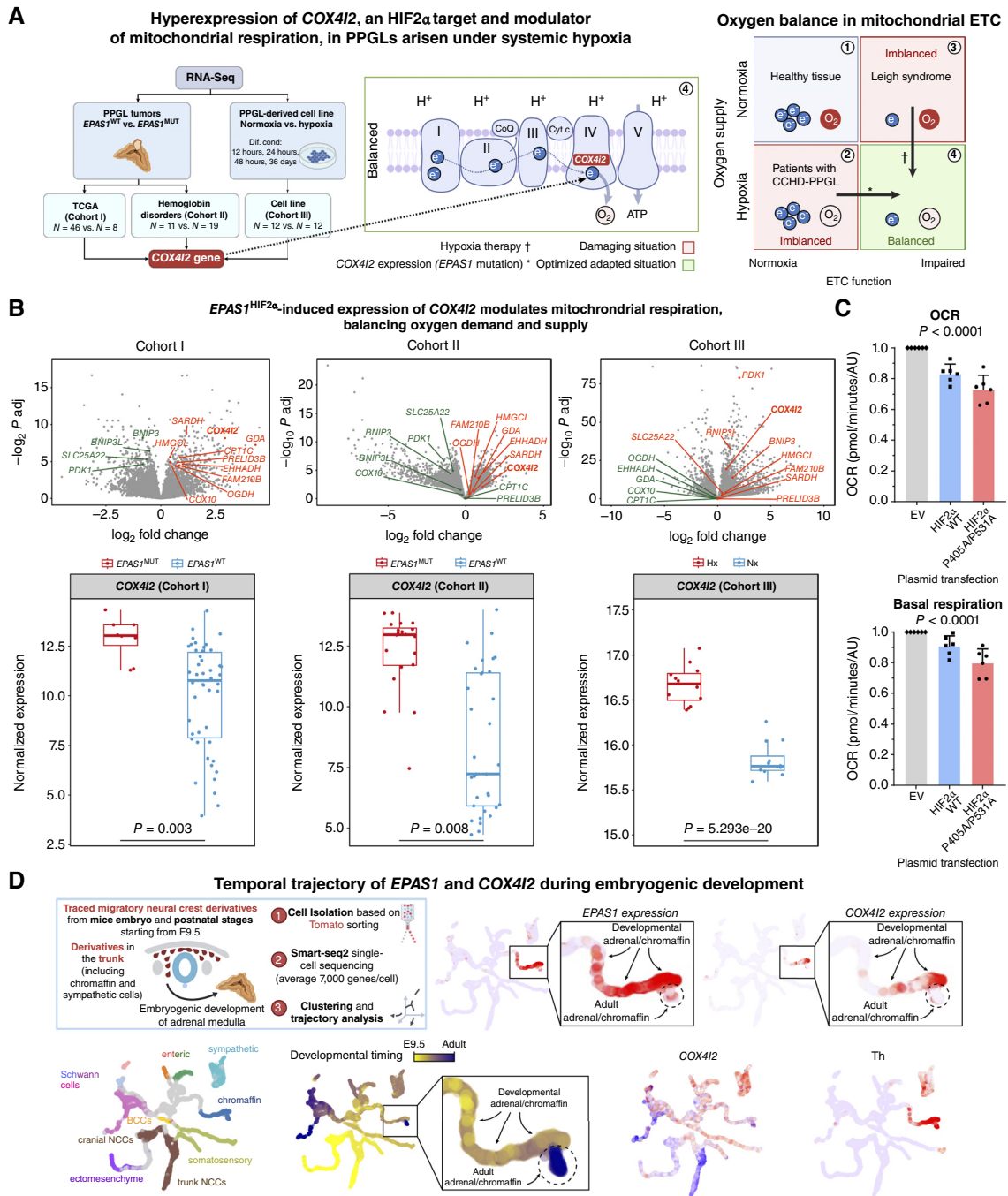


**Figure 4.** Transcription analyses for functional and developmental insights of *EPAS1* in PPGL tumorigenesis. **A**, Workflow of bulk RNA-seq data analysis using three different cohorts: cohort I comprised non-CCHD sympathetic PPGL tumors: WT ( $n = 46$ ) or mutated ( $n = 8$ ) for *EPAS1* (61, 65); cohort II comprised sympathetic PPGL tumors from patients with hemoglobin disorders: 11 tumors *EPAS1*<sup>WT</sup> and 19 tumors *EPAS1*<sup>MUT</sup> (59); cohort III comprised PPGL-derived cell line that we cultured under normoxic and hypoxic conditions for 12, 24, and 48 hours and 36 days (three replicates for each condition, 12 samples in normoxia and 12 in hypoxia). Of the 354 genes that were differentially expressed in patients with PPGL tumors, 14 mitochondrial genes were found, of which one was *COX4I2*, the less common isoform of COX (mitochondrial respiratory complex 4) and the terminal electron acceptor of the oxidative phosphorylation system. **B**, Top part: Volcano plots of the differentially expressed genes between *EPAS1*<sup>MUT</sup> and *EPAS1*<sup>WT</sup> tumor samples from cohorts I and II, and between hypoxia and normoxia conditions in cohort III. Fourteen differentially expressed mitochondrial genes are highlighted (upregulated genes in orange color, downregulated genes in green color). Bottom part: normalized expression of *COX4I2* in cohorts I, II, and III. **C**, Mitochondrial respiration using Seahorse equipment ( $n = 6$ /group; mean  $\pm$  SEM) in stable cell line HEK293T expressing empty vector (EV)-Control, HIF2 $\alpha$ <sup>WT</sup>, and mutant HIF2 $\alpha$ <sup>P405A/P531A</sup> through plasmid transfection. Oxygen consumption respiration (OCR; top), basal respiration (bottom). **D**, scRNA-seq data comprising the entire tree of neural crest lineage development, which includes differentiation trajectory from the neural crest toward chromaffin cells via Schwann cell precursor and bridge-state intermediates (89). The scRNA-seq data show that *EPAS1* and *COX4I2* expression are upregulated during development and downregulated in postnatal chromaffin/adrenal medulla cells, after the onset of breathing. BCCs, boundary cap cells; NCCs, neural crest cells; Th, tyrosine hydroxylase (chromaffin cell marker). (**A**, Created with BioRender.com and **D**, Schematic of scRNA-seq was created with BioRender.com.)

Downloaded from <http://aacrjournals.org/cancerdiscovery/article-pdf/doi/10.1158/2159-8290.CD-24-0943/3557533/CD-24-0943.pdf> by guest on 10 April 2025

under normoxia); and 149 patients with CCHD plus PPGL (tumors developed under hypoxia; Fig. 5A). PPGLs were the only tumors enriched in CCHD, consistent with the findings of previous epidemiological studies (54, 55). We collected and analyzed clinical data regarding (i) heart disease, such as the CCHD type and heart surgery; (ii) hypoxia exposure, such as the timing of hypoxia initiation and duration, and O<sub>2</sub> saturation (SatO<sub>2</sub>); and (iii) PPGLs, such as the age at diagnosis, tumor type, tumor multiplicity, metastatic status, and biochemical and genotype profiles.

To identify a potential time window for systemic hypoxia effects, we analyzed clinical outcomes of two patient groups with CCHD with PPGLs: one with severe heart complications causing hypoxia since birth and the other with Eisenmenger syndrome, a rare heart defect that causes blood vessel damage, pulmonary hypertension, and systemic hypoxia that can start not right after birth but during childhood or early adulthood (94). In the first group, 56/66 (85%) patients with hypoxia since birth developed catecholamine-secreting PPGL tumors originating in sympathetic system cells, such as the adrenal medulla and/or paraganglia (Fig. 5B and C; Supplementary Table S12). The remaining 10/66 (15%) patients were diagnosed with biochemically silent PPGLs originating within parasympathetic paraganglia, invariably carotid body tumors. By contrast, patients in the second group, with childhood/early adult hypoxia onset, presented the opposite profile, with 7/11 (64%) parasympathetic carotid body tumors and 4/11 (36%) sympathetic tumors (Fig. 5B and C; Supplementary Table S12). This result suggests for an early time window to the tumorigenic effect of hypoxia in the sympathetic system, possibly while the adrenal medulla and paraganglia are still uninnervated, developmentally immature, and sensitive and autonomously responsive to low oxygen levels (17, 18).

### Influence of Oxygen Levels on Tumor Development

We examined differences between patients with CCHD who developed PPGLs ( $N = 149$ ) and those who did not ( $N = 1,599$ ), delving into the analysis of patients with reported SatO<sub>2</sub> levels. The former group had significantly lower SatO<sub>2</sub> than patients with CCHD without PPGLs (average SatO<sub>2</sub>: 81.2%, range: 68%–91% vs. average SatO<sub>2</sub>: 83.2%, range 69%–91%, respectively;  $P = 0.01$ ; Fig. 5D; Supplementary Table S13). Analyzing the subgroup of patients with CCHD who were not subjected to cardiac surgery, which more accurately represented the natural disease history, yielded similar results. Unoperated patients with CCHD who developed PPGLs had an average SatO<sub>2</sub> of 79.3% (range: 68%–90%), whereas unoperated patients with CCHD without PPGLs had an average SatO<sub>2</sub> of 83.4% (range: 73%–91%;  $P = 0.0003$ ; Fig. 5E; Supplementary Table S13). These data provide clinical support for the general but largely untested assumption that systemic hypoxia and different SatO<sub>2</sub> levels could affect human tumorigenesis (95, 96).

### Influence of Early Hypoxia Correction on Tumor Development

We observed a significant distinct surgical status within the CCHD cohort that developed PPGL tumors compared with that which did not. Although 1,204/1,368 (88%) of

patients with CCHD without PPGL underwent early complete heart repair surgery, which indicated a return to normoxic conditions, only 13/75 (17%) patients with CCHD who developed PPGLs underwent complete heart repair surgery (Fig. 5F;  $P < 0.001$ ; Supplementary Table S14). Most patients (62/75, 83%) who developed PPGLs did not undergo surgery for heart disease, which implies that they maintained some degree of hypoxia throughout their lives or were offered only a palliative medical intervention that did not reverse hypoxia (Fig. 5F; Supplementary Table S14). This may suggest that early complete heart surgery, which brings SatO<sub>2</sub> to normal levels, could act as a protective factor against tumor development.

Altogether, this analysis revealed both tissue and time dependency of hypoxia in tumorigenesis. Tissue dependency is related to the observation that patients with systemic hypoxia are enriched with tumors occurring exclusively in hypoxia-sensing and reacting cells, such as the carotid body, paraganglia, and adrenal medulla. Time dependency relates to hypoxia diagnosed since birth, favoring sympathetic PPGL development, whereas delayed hypoxia favors parasympathetic PPGL tumor (carotid body tumors) development. Our results also suggest that early surgical heart correction, which restores normoxia, may protect against PPGL development.

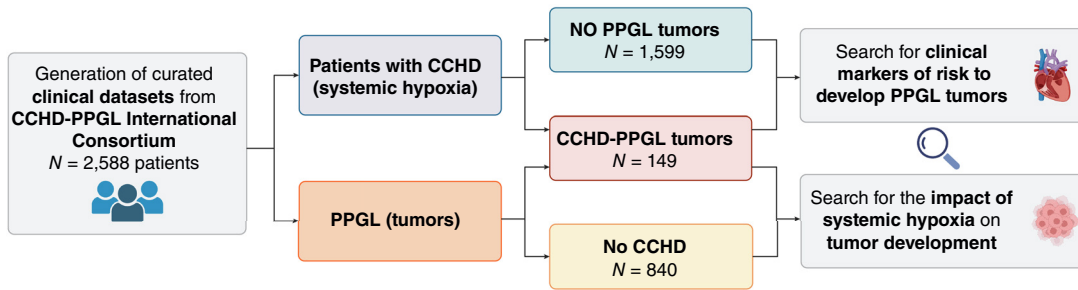
### Influence of Systemic Hypoxia and *EPAS1*-Enriched PPGLs on Long-term Tumor Features

To investigate systemic hypoxia effects on human tumor characteristics, we compared clinical features of 989 patients with PPGLs, with ( $N = 149$ ; CCHD-PPGLs) or without ( $N = 840$ ; non-CCHD-PPGLs) congenital systemic hypoxia. Although the formal genetic status was not always determined to this extended cohort, based on the high *EPAS1* mutation frequency identified in our cohort with tumor samples available (Fig. 1A), most patients with CCHD with sympathetic PPGL were assumed to have *EPAS1*<sup>MUT</sup> tumors. Compared with patients with PPGL but without systemic hypoxia, those with CCHD-PPGL were younger at the time of PPGL diagnosis (odds ratio, OR = 0.92; confidence interval, CI, 0.91–0.94;  $P < 0.001$ ), presented more frequently with paragangliomas than pheochromocytomas (OR = 9.98, CI, 6.19–16.11;  $P < 0.001$ ), and were more likely to have multiple PPGL tumors (OR = 1.99, CI, 1.17–3.25;  $P = 0.008$ ). Although PPGLs are usually nonmetastatic tumors, patients with CCHD were at substantially increased risk of developing metastatic disease compared with those without CCHD who were diagnosed with PPGL (OR = 2.34, CI, 1.11–4.59;  $P = 0.018$ ; Fig. 6A and B; Supplementary Tables S15 and S16). These results indicate that systemic hypoxia increases the risk of developing PPGLs and modulates tumor phenotypes, being associated with greater aggressiveness and metastatic risk.

## DISCUSSION

Our study presents *EPAS1* as a fundamental driver of evolutionary adaptation to systemic hypoxia, evident across extremely diverse conditions such as in populations living

### A Analyzing clinical cohorts to assess the temporal and tissue-specific effects of systemic hypoxia on human tumorigenesis



### B Higher incidence of *EPAS1*<sup>MUT</sup> PPGL sympathetic tumors in individuals with systemic hypoxia since birth, whereas early hypoxia correction is associated with a decreased tumor risk

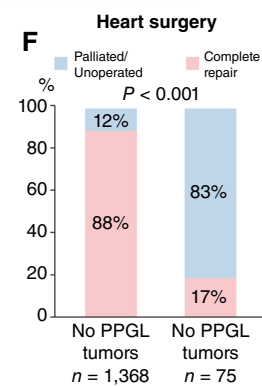
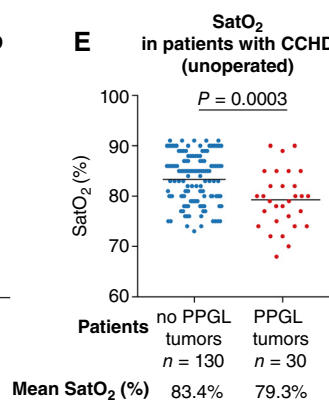
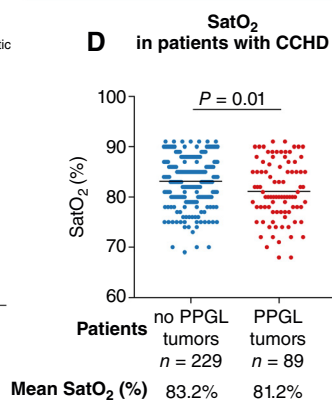
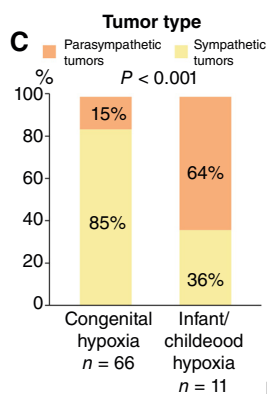
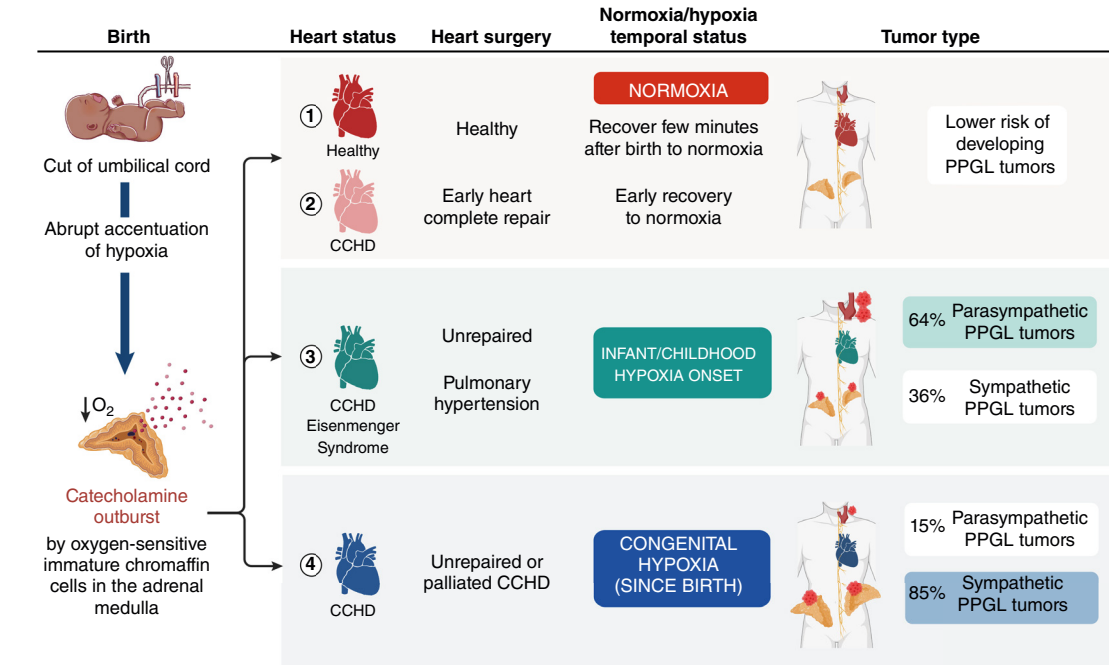
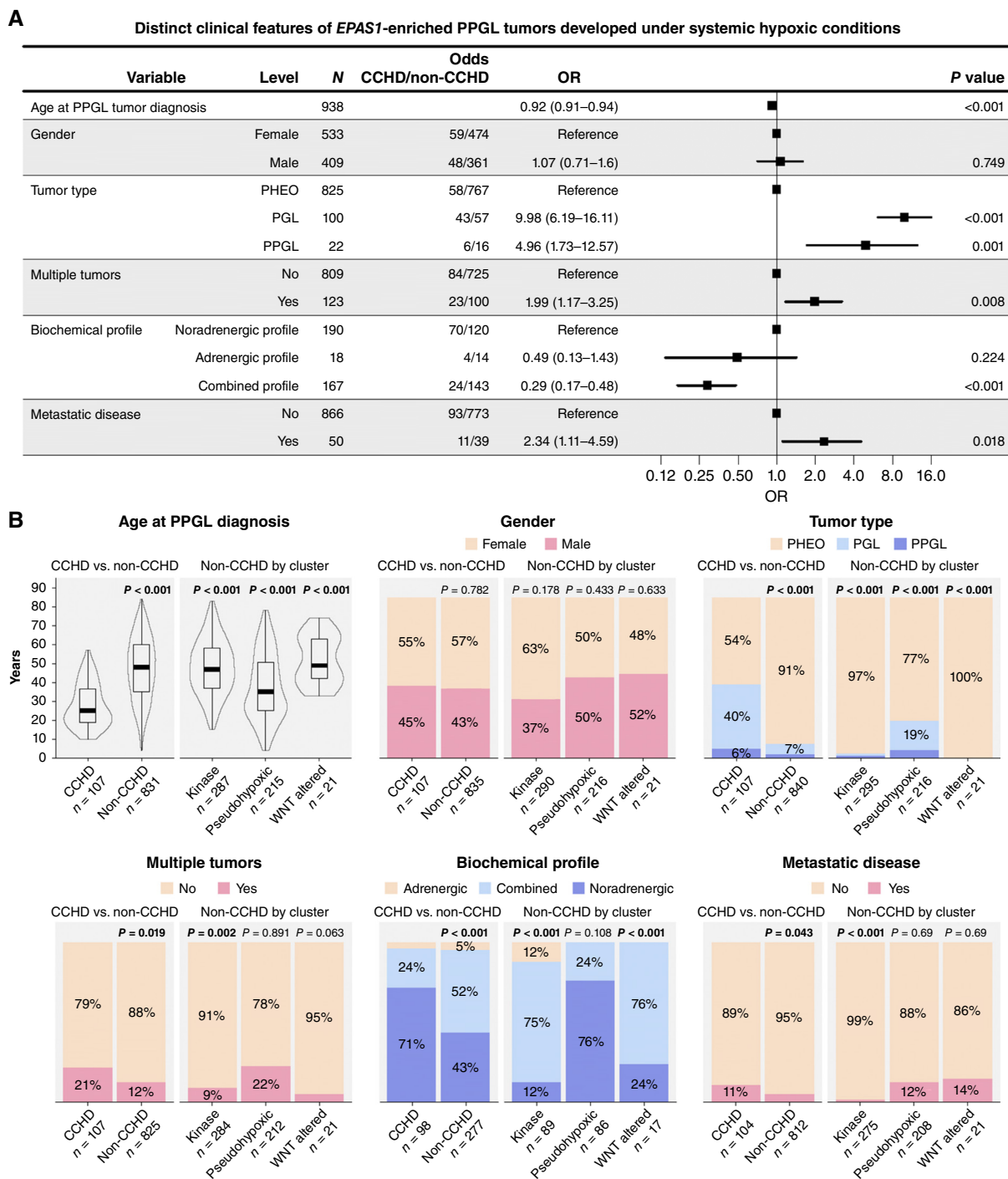


**Figure 5.** Temporal and tissue-specific impact of systemic hypoxia in tumorigenesis, and the influence of oxygen levels and early hypoxia correction. **A**, Overview of clinical datasets collected from the CCHD-PPGL International Consortium for the study. Clinical features from 2,588 patients have been collected and curated, involving patients with CCHD without PPGL tumors ( $N = 1,599$ ), patients with CCHD-PPGL ( $N = 149$ ), and patients with PPGL without CCHD ( $N = 840$ ). Analyzing patients with CCHD with or without PPGL tumors (with systemic hypoxia in a determinate moment of their lives) involved investigating clinical markers for the risk of developing PPGL tumors. Clinical characteristics from patients with PPGL tumors with or without CCHD were interrogated to determine the impact of systemic hypoxia on tumor development. **B**, Schematic figure depicting the hypoxia levels of patients with CCHD in their life and catecholaminergic system. Depending on their systemic hypoxia, they are more prone to develop PPGL tumors. **C**, PPGL tumor types depending on the hypoxia exposure time. **D**, Oxygen saturation (%) in patients with CCHD with or without PPGL tumors. **E**, Oxygen saturation (%) in unoperated patients with CCHD with and without PPGL tumors. **F**, CCHD surgical management type and occurrence of PPGL tumors.  $\text{SatO}_2$ , oxygen saturation. (**A** and **D**, Created with BioRender.com.)



Downloaded from <http://aacrjournals.org/cancerdiscovery/article-pdf/doi/10.1158/2159-8290.CD-24-0943/3557533/04-24-0943.pdf> by guest on 10 April 2025

**Figure 6.** Hypoxic impact in PPGL tumor development: clinical features comparison of patients with CCHD-PPGL and without CCHD-PPGL (non-CCHD-PPGL). **A**, Univariate regression model (odds ratio, OR) of patients with PPGL and CCHD-PPGL. **B**, Representation of clinical variables in patients with PPGL and CCHD-PPGL.

in high-altitude hypoxia (22–30) and during human tumor development under early and prolonged systemic hypoxia (Fig. 1D). The findings of this study broaden our knowledge of the biological connectivity degree of life. This previously unreported broad convergence level suggests that other relevant molecular adaptation mechanisms occurring in natural

populations may play a role in tumors facing similar stressors (Supplementary Fig. S7A–S7E). Hence, future projects could investigate roles of genes selected in populations adapted to high UV in skin melanomas or the impact of genes selected in populations adapted to dietary restrictions (amino acids, fat, and carbohydrates) on tumor metabolism reprogramming.

Overall, harnessing adaptation mechanisms in natural populations could open new avenues for enhancing the detection of cancer vulnerabilities and therapies.

Our study also describes various significant correspondences occurring in high-altitude populations and tumors developed in systemic hypoxia, such as accelerated adaptability, gene functional plasticity, and embryological and tissue-dependence effects of hypoxia stress.

### Accelerated Adaptability

Accelerated adaptability mechanisms, such as increased mutability and advantageous genetic allele exchange between different species (adaptive introgression), have been observed in cell lines cultivated in hypoxia (79–83) and in animals and human populations adapted to high altitudes (35–38). These processes culminate in a genetic pool to cope with the effects of low oxygen levels. We found that human tumors developed under hypoxia also underwent accelerated adaptability, with *EPAS1* mutations as tumorigenesis drivers. Our data suggest that this highly specific and multistep process is associated with decreased DNA repair in sympathetic nervous system cells, whereas healthy tissues surrounding PPGLs from patients with CCHD, such as fat, stroma, and adrenal cortex tissues, retain detectable DNA repair proteins (Fig. 2A). After this, sympathetic cells acquire genomic instability and somatic mutations, indicated by the increased TMB (Fig. 2D–F). In this context, a mutation occurring in the *EPAS1* oxygen-sensing domain undergoes extreme positive selection (Supplementary Fig. S10). Our analysis of the tumor evolutionary history via calculating CCF localized *EPAS1* as a tumor-initiating mutation (trunk mutation) and an oncogenic driver of PPGL development under hypoxia (Fig. 1C). For unknown reasons, this process is restricted to sympathetic tissues (adrenal medulla and paraganglia) composed of cells still immature at birth, capable of sensing hypoxia, and promoting surges in catecholamine secretion (17, 18, 97–100).

### Positive Selection of *EPAS1* Genetic Variants Exclusively in High-Altitude and Systemic Hypoxia-Developed Tumors

We found that the positive selection of *EPAS1* genetic variants was exclusive to hypoxic conditions. They have reportedly undergone one of the strongest selections observed in highlander Tibetans and Sherpas with a 90% frequency and fixation index ( $F_{st}$ ) reaching 0.81 (22, 23, 25). In parallel, tumors developed under systemic hypoxia harbored >90% of *EPAS1* mutations (Fig. 1A and D). This strong evolutionary process, known as *selective sweep*, has also been described in highlander populations across different species living at high altitudes, such as horses (26), dogs (27), wolves (28), pigs (29), and ducks (30). By contrast, *EPAS1* variants are infrequent or nonexistent in populations living at low altitudes or in tumors of patients with normoxia (Fig. 1D; Supplementary Figs. S7A–S7E and S8; Supplementary Tables S6 and S7).

### Functional Plasticity

Although the positive selection of high-altitude adaptation and sympathetic tumor genomes developed under systemic hypoxia converge on *EPAS1*, selected variants have distinct

characteristics and confer opposite molecular consequences. Although Tibetans and Sherpas are enriched in noncoding variants located in the promoter region with a loss-of-function effect (31–33), we showed that tumors developed under hypoxia carried specific missense mutations in the oxygen degradation domain (amino acids 529–542) that conferred resistance to VHL-dependent protein degradation, leading to gain-of-function and oncogenic effects (Supplementary Fig. S17; refs. 40, 48, 101). Missense mutations outside the oxygen degradation domain, that is, the Andean H194R variant, have also been shown to be inactivated and positively selected at high altitudes (34). These differing effects uncover functional plasticity of HIF2 $\alpha$ -related adaptations and survival to hypoxia.

Hypoxia is regulated by HIFs, comprising inducible and constitutive subunits. In normoxia, hydroxylation of specific prolines in HIF $\alpha$  units (Pro531 in HIF2 $\alpha$  and Pro564 in HIF1 $\alpha$ ) signals oxygen sufficiency and causes VHL-dependent ubiquitination and proteasome-mediated degradation (7, 9, 10). This hydroxylation does not occur in hypoxia, hence pleiotropically activating HIF $\alpha$ , mediated via transcriptional upregulation of numerous target genes involved in several pathways. HIF2 $\alpha$  controls EPO expression (20, 21), which is important because although lowlander sojourners visiting high altitudes experience rapid increases in EPO and hemoglobin concentrations to compensate for acute hypoxia, high hemoglobin levels are detrimental in the long term because they cause blood viscosity that paradoxically causes poor oxygenation and recurrent abortions, thus decreasing reproductive fitness. Hence, *EPAS1* gene variants positively selected in humans and other animals from the Tibetan region hamper HIF2 $\alpha$  activation, which decreases hypoxia response, reduces EPO production, and lowers hemoglobin concentration, enabling their survival and reproduction in high altitudes. Therefore, Tibetan women carrying *EPAS1*<sup>LOF</sup> alleles present lower hemoglobin levels and a greater capacity to carry pregnancies to completion, explaining the observed selection sweep (Supplementary Fig. S17; refs. 102, 103). The link between Tibetan *EPAS1*<sup>LOF</sup> alleles and higher reproductive fitness under chronic hypoxia has been confirmed in genetically edited mice (104).

Contrary to HIF2 $\alpha$ -hampering genetic variants selected in highlanders, *EPAS1* mutations detected in PPGL tumors strongly activate HIF2 $\alpha$  via affecting the HIF2 $\alpha$  Pro531 hydroxylation site or neighboring residues at the oxygen-dependent degradation domain, impeding its VHL-mediated proteasome degradation (40, 48, 101). We have previously shown that these *EPAS1*-activating mutants are stable in normoxia, triggering expression of genes associated with cell differentiation and stemness, which increase the tumor growth capacity in xenografts (40). Furthermore, these *EPAS1*<sup>GOF</sup> mutants become further stabilized and activated when oxygen levels reduce from 21% to 1%, suggesting that they probably yield additional survival advantages under hypoxia (40). The 20-fold increase in *EPAS1*<sup>GOF</sup> mutation frequency seen in normoxic PPGLs (non-CCHD related) to hypoxic PPGLs (patients with CCHD, 4.5%–89%; Fig. 1D) strongly suggests that *EPAS1*<sup>GOF</sup> confers increased fitness to sympathetic chromaffin cells, which may favor tumor development (Supplementary Fig. S17).

## Time- and Tissue-Dependent Tumor Risk of Systemic Hypoxia

Hypoxia is a prevalent environmental stressor contributing to morbidity and mortality in humans and marine life (105–108). Adult-onset hypoxia is estimated to affect approximately a billion people with obstructive sleep apnea and 400 million people with chronic obstructive pulmonary disease worldwide (109); at birth, hypoxia affects more than 80 million people living above 2,500 m (110), and 1 to 2 infants per 1,000 live births have CCHD (111). Hypoxia at birth has been linked to a sixfold increased risk of PPGLs, whereas no other tumor type is enriched to the same degree (54, 55). These observations are consistent with independent experimental data from William G. Kaelin (Dana-Farber/Harvard Cancer Center in Boston, MA, USA) and Sir Peter J. Ratcliffe (University of Oxford and the Francis Crick Institute in the UK), who suggested that PPGL tumor development was promoted by defective adrenal development and developmental apoptosis (112, 113). Our results clearly show a distinct effect of systemic hypoxia when it starts from birth compared with afterward during childhood. Patients with CCHD and systemic hypoxia since birth were enriched in sympathetic catecholamine-secreting tumors, consistent with the early impact of systemic hypoxia on developmentally immature cells from the adrenal medulla and paraganglia of babies. During human fetal development, the environment is characterized by significant hypoxemia, with  $O_2$  pressures as low as 20 mm Hg (114), lower than that encountered by climbers at the Everest summit at 8,850 m (25–28 mm Hg; refs. 115, 116). It further decreases immediately after birth following umbilical cord clamping (Fig. 5B; ref. 97). At birth, immature chromaffin cells in the adrenal medulla sense an abrupt decline in oxygen levels, triggering an extraordinary surge in catecholamine production, reaching up to 100-fold higher than those in a resting adult (18, 98–100). This surge shields infants from hypoxia-induced harm and mortality, prompting essential physiological responses, including heightened breathing, heart rates, and cardiac output. These responses work in tandem with blood flow redirection to critical organs, such as the heart and brain. Consequently, healthy newborns attain normoxia within 3 to 5 minutes after birth (97). Approximately 1 week after birth, these cells mature, become innervated by splanchnic nerves, and lose their initial oxygen sensitivity. However, infants born with CCHD continue to experience hypoxemia because the defective heart chambers contain a mixture of oxygenated and deoxygenated blood.

By contrast, patients with CCHD and systemic hypoxia occurring later in childhood present proportionally fewer sympathetic lesions, in line with the time-specific oncogenic effect of systemic hypoxia and sympathetic PPGL tumor development. These patients are proportionally enriched with carotid body tumors, possibly the result of disrupted adaptation (or maladaptation) to systemic hypoxia exposure at any time during their lifespan, rather than a true tumorigenic process. The carotid body, sympathetic paraganglia, and adrenal medulla are dependent on HIF2 $\alpha$  for their embryological development and physiological function in adults (Supplementary Fig. S18A–S18C; ref. 14).

Patients with hypoxia and CCHD exclusively have a sixfold increased risk of developing PPGL tumors (54, 55); the cause remains unknown. PPGLs are neural crest tumors derived from hypoxia-sensing and responsive cells of the adrenal medulla and sympathetic and parasympathetic paraganglia (14). Our data showed that in addition to tumor type exclusivity, CCHD-PPGL is also a nearly genetically exclusive disease with *EPAS1* gene convergence. This clinical and genetic exclusiveness is probably a reflection of the unique embryological role and expression pattern of *EPAS1* itself (14, 117, 118). Although HIF1 $\alpha$  appears early in evolution and is expressed ubiquitously, HIF2 $\alpha$  arises later in evolution because of gene duplication, and its embryonic and adult gene expression remains primarily restricted to few cell types, but prominently autonomic lineage cells, that is, cells driving the normal development of the carotid body (parasympathetic) and sympathetic tissues, the organs that later will undergo tumorigenesis (Supplementary Fig. S19).

## Oxygen Consumption and Supply Balance as an Advantageous Mechanism for Survival and Proliferation

Our results, obtained via oxygen consumption rate measurements in cell lines with constitutively expressed *EPAS1* mutations, transcriptomic profiling of *EPAS1*-mutant PPGLs, and rat cell lines exposed to hypoxia, offer compelling evidence that *EPAS1* modulates the ETC via regulating the atypical *COX4I2* isoform expression (Fig. 4A). These findings suggest that reduced ETC activity, which was previously observed *in vitro* under hypoxic conditions (90), also occurs in tumors with *EPAS1* mutations that thrive in hypoxic environments. These observations suggest a potential mechanism that challenges the conventional understanding of *EPAS1*<sup>MUT</sup> PPGL survival under low-oxygen conditions. Instead of enhancing the ETC to maximize use of all available oxygen molecules in hypoxia to produce 30 ATP molecules via mitochondrial respiration, our data suggest that the competitive edge in survival and proliferation observed in *EPAS1*<sup>MUT</sup> tumors arises from efficient matching of the ETC with available oxygen supply (Fig. 4A; Supplementary Fig. S16). This balance in the ETC and oxygen use, achieved via slowing down the ETC under hypoxic conditions, likely reduces the toxicity associated with an imbalance between ETC activity and oxygen supply, as observed in hypoxic and superoxic conditions. Similar findings regarding the beneficial effects of balancing oxygen consumption and supply have been reported in Leigh mitochondrial disease, which is caused by mutations that impair the ETC. When knockout mice for *Ndufs4*, a common cause of Leigh syndrome, were exposed to moderate hypoxia (11%  $O_2$ ), their survival rates were found to increase significantly, whereas moderate hyperoxia (55%  $O_2$ ) led to early deaths (119). Hypoxia treatment also provided substantial protection and extended the survival of another Leigh-like mouse model with a *SDHC* homozygous knockout (120). Heterozygous *SDHC* mutations predispose humans to PPGL (121).

## Translation to the Clinic

The dependency on HIF2 $\alpha$  in PPGLs presents a promising therapeutic opportunity with HIF2 $\alpha$  inhibitors currently under clinical investigation. The NCT04924075 trial

(Cohort A1), evaluating belzutifan in unselected metastatic PPGLs, has completed enrollment of around 150 patients, with results expected soon. Separately, the NCT04895748 trial investigates another HIF2 $\alpha$  inhibitor, DFF332, for renal cell carcinoma and selected metastatic PPGL cases with hypoxia pathway mutations, including *EPAS1*.

Our *in vitro* studies on HEKT293 cells expressing either WT *EPAS1* or the double mutant p.P405A/P531A allele revealed a proliferative advantage in mutant cells, consistent with an *EPAS1* oncogenic role (40). Treatment with 100  $\mu$ mol/L belzutifan over 24 to 72 hours showed increased sensitivity in *EPAS1*-mutant cells, as shown in Supplementary Fig. S20A–S20H. Case reports further support belzutifan's potential for *EPAS1*-mutant PPGLs. One report documents a patient with mosaic c.1589C>A (p.A530E) *EPAS1* mutation and five PPGLs who achieved a 50% tumor reduction and normalized catecholamine levels with 120 mg belzutifan daily, sustained for nearly 2 years (122). Another case series describes two patients with PPGL with somatic *EPAS1* p.A530V mutations treated with 80 mg belzutifan, both experiencing rapid normalization of catecholamine markers and resolution of hypertension and tachycardia (123). Together, these findings and case reports suggest belzutifan as a promising therapy for *EPAS1*/HIF2 $\alpha$ -driven PPGLs.

An additional strategy for hypoxia-driven PPGLs with DNA repair deficiencies, including reduced PARP1 in hypoxic PPGL cells (Fig. 3A and B), involves PARP1 inhibitors, which could push tumor cells toward lethal DNA damage accumulation. The phase II trial NCT04394858 is currently recruiting unselected metastatic PPGL patients to assess the efficacy of combining olaparib with temozolomide.

## Leveraging Adaptation Mechanisms in Natural Populations and Tumors

Over the past decades, multiomics studies and genetically engineered preclinical models have contributed to elucidate cancer vulnerabilities amenable to therapeutic intervention. Nevertheless, the rising global incidence of cancer, coupled with persistent challenges in achieving effective treatment outcomes underscore the urgent need for innovative, multidisciplinary strategies to enhance therapeutic efficacy and improve patient outcomes. Our work highlights the impact of the *EPAS1* gene on driving adaptation to hypoxic environments in both natural populations and in cancers, emphasizing its dual role in evolution and cancer biology. This finding raises the compelling possibility that other genes conferring adaptive advantages in specific natural stress scenarios, such as high UV exposure and nutrient (glucose, lipid, and amino acid) or mineral (iron, magnesium, and zinc) scarcity may also play key roles in cancer processes such as tumor initiation, metastasis, and/or therapeutic resistance. Leveraging adaptation mechanisms observed in natural populations may provide innovative strategies for identifying cancer vulnerabilities and developing effective therapies.

## Conclusions

The genetic architecture of high-altitude populations is shaped by a strong positive selection of the *EPAS1* gene, encoding HIF2 $\alpha$  (22–30, 35, 36). We generated and integrated

multilayered hypoxia data from large clinical datasets, multiomics analyses of tumors, and *in vitro* experiments. We found evidence of the highly specific effects of systemic hypoxia on tumorigenesis in tissue, time, and oxygen level-dependent manners. Tumors from patients born with cardiac abnormalities resulting in chronic systemic hypoxemia parallels the genetic adaptation mechanisms observed in high-altitude dwellers harboring highly prevalent *EPAS1* genetic variants. Mechanistically, our data support an intricate tumorigenesis model in which systemic hypoxia deregulates the DNA repair machinery of hypoxia-sensitive and responsive cells, thereby increasing their genetic pool of CN alterations and mutations. In this state of genomic instability, we propose that *EPAS1* mutations promote oxygen consumption rate optimization via expressing the atypical isoform *COX4I2*. This study provides clinical, evolutionary, and mechanistic insights into the effects of chronic hypoxia on tumorigenesis, and the unprecedented parallelism of genetic adaptations to hypoxia in two widely different contexts: in high-altitude dwellers and tumors developed under systemic hypoxia.

## METHODS

### Experimental Design

In this study, we aimed to characterize the level of genetic adaptive parallelism among two very distant hypoxic conditions, such as high-altitude populations of the Himalayas (i.e., Sherpas and Tibetans) and hypoxia-sensing cells of the body that are prone to develop PPGL tumors when exposed to prolonged hypoxia due to a congenital blood-mixing heart defect (CCHD). We also aimed to characterize in deep the molecular mechanism underlying hypoxia-driven tumorigenesis in humans. To be able to tackle these goals, we generated and analyzed multimodal data from clinically informative hypoxic and normoxic patients; high- and low-altitude populations; genetic and genomic profiles of human tumors; status of DNA repair system in the tumors; bulk transcriptomic profiles of human tumors and cell lines cultivated in normoxia and hypoxia; single-cell transcriptomic profiles of the developmental trajectory of the hypoxia-sensing cells of the body; and *in vitro* experiments to assess the downstream effect of *EPAS1* in cellular respiration rate and oxygen balance.

All multimodal data generated and/or analyzed in this study are available through publicly accessible data repositories (see “Data Availability” section) and/or included in the Supplementary Tables.

### Ethical Committee

This study was conducted in accordance with the ethical principles of the Declaration of Helsinki and with the approval for research granted by the Ethics Committee from the Vall d'Hebron University Hospital (Barcelona, Spain; PR(AG)158/2018); La Paz University Hospital (Madrid, Spain; PI-3230); Central University Hospital of Asturias (Oviedo, Spain; CEImPA 2020.547); Assistance Publique–Hôpitaux de Paris (Paris, France; #00011928); The University of Texas Health Science Center at San Antonio (San Antonio, TX, USA; IRB #HSC06-069H.); Mayo Clinic (Rochester, MN, USA; 14-008336); Brigham and Women's Hospital, Harvard Medical School (Boston, USA; 2013P000564); and others. The research was conducted in accordance with local data protection laws, and all patients provided written informed consent. All data provided is anonymized in line with applicable laws and regulations.

### Cohort of CCHD-Only, PPGL-Only, and CCHD-PPGL Patients

To generate data for the analysis of the potential impact of systemic hypoxia on the risk of developing tumor, on tumorigenesis, and on the modulation of phenotypic characteristics of the tumors, we needed large and informative cohorts of patients with and without PPGL tumors and with and without systemic hypoxia. To obtain such cohorts, we established a multidisciplinary International Consortium comprising clinicians (cardiologists, endocrinologists, oncologists, and radiologists), pathologists specializing in endocrine tumors, genomic researchers, and molecular researchers from 39 institutes across five countries. Many of these members are part of the European Network for the Study of Adrenal Tumours (ENS@T; <https://ensat.org/>) and the American Australian Asian Adrenal Alliance (A5; <https://adrenal-a5.org/>) and have been engaged in PPGL and hypoxia research for decades. Clinical data were generated and curated from 2,854 patients with informative clinical conditions for the study, such as 1,599 patients with CCHD but not PPGL; 840 patients with sympathetic PPGL but not CCHD; 266 patients with parasympathetic PPGL (all carotid body tumors) but not CCHD [ $n = 52$  (63),  $n = 24$  (64), and sequenced data kindly shared by Mercedes Robledo's lab ( $n = 190$ )]; and 149 patients with CCHD-PPGL, which is a substantial number due to the rarity of the combined CCHD-PPGL condition. Detailed information about the patients is provided in Supplementary Tables S1 and S6.

### Cardiac and Endocrine Features of the Cohorts

The inclusion criteria for the CCHD cohorts were patients with CCHD with cyanosis defined as resting arterial oxygen saturation below 92%. Patients were divided by cardiac anatomy in six groups: functionally univentricular heart; transposition of the great arteries; tetralogy of Fallot, including pulmonary atresia with ventricular septal defect; pulmonary atresia with intact ventricular septum; ventricular septal defect; and others (Supplementary Table S1). According to the 32nd Bethesda Conference classification (124), 66.7% of patients had a CCHD of great complexity. More than half of the cohort was either unoperated or only underwent a palliative procedure, resulting in a majority of patients who had been cyanotic for decades. None of the patients with CCHD with PPGL had a family history of PPGL-related hereditary syndromes. The diagnosis of pheochromocytoma and paraganglioma was confirmed by histologic confirmation and/or symptoms, altered biochemical parameters, and imaging findings, as indicated by the guidelines (125). The biochemical profile of the tumors was determined by standard catecholamine measurements in the plasma (Supplementary Table S1).

### Search for Risk Factors Associated with Tumor Formation and Tumor Phenotypic Variation

We searched whether clinical factors linked to hypoxia were potentially associated with increased risk to develop PPGL tumors and/or tumor aggressiveness. Using Mann–Whitney  $U$  test, we compared the tumor type (sympathetic/parasympathetic lineage) developed in patients with congenital hypoxia ( $n = 66$ ) or infant/childhood hypoxia ( $n = 11$ ). We also compared the oxygen saturation levels and status of normoxia correction by heart surgery in patients with CCHD who did not develop and those who did develop PPGL tumors ( $N = 229$  vs.  $N = 89$  patients and  $N = 1,368$  vs.  $N = 75$ , respectively).

To test whether clinical factors linked to hypoxia were potentially modulating phenotypic characteristics of PPGL tumors, we performed a set of univariate binominal generalized lineal models to compare the following attributes: (i) age at PPGL diagnosis, (ii) gender (two levels: male and female), (iii) tumor type (three levels: PHEO, PGL, and PPGL), (iv) multiplicity (two levels: yes and no),

(v) biochemical profile (three levels: noradrenergic, adrenergic, and combined), and (vi) metastasis (two levels: yes and no) in patients who had developed PPGL tumors in a context of systemic normoxia (non-CCHD) or systemic hypoxic (CCHD). Similar analyses were performed separating the PPGLs by molecular clusters (pseudohypoxia, kinase, and WNT cluster). As all analyses generated 24 different generalized lineal models, the results were correct for multiple testing and  $P$  values were adjusted by controlling the FDR (126). The abovementioned analyses are graphically illustrated in Fig. 6A and B; Supplementary Tables S15 and S16.

### Statistical Analysis

Percentages and frequencies are presented for qualitative variables and  $\chi^2$  or Fisher test was used for comparisons. Means (SDs) and medians (25th and 75th percentiles) were calculated for quantitative variables, and Mann–Whitney  $U$  test or Kruskal–Wallis test was used for comparisons depending on the number of groups. All statistical analyses were performed using the R software, version 4.3.1 (R Core Team, RRID:SCR\_001905). GraphPad Prism 6 (RRID:SCR\_002798) software was used for graphical presentation of the data.

### Biological Samples from CCHD-PPGL and Parasympathetic PPGL Tumors

Biological samples for genetics analysis were obtained through the CCHD-PPGL International Consortium. In total, 27 patients diagnosed with CCHD (22 newly recruited patients and five from Vaidya and colleagues; ref. 56) developed 28 sympathetic PPGLs, including 14 pheochromocytomas (adrenal medulla), 14 thoracic/abdominal paragangliomas (12 abdominal retroperitoneal, one thoracic mediastinal, and one retroperitoneal vesical), and 9 parasympathetic head and neck paragangliomas, all carotid bodies (CB). Twenty patients presented with a solitary tumor and seven with multiple and independent tumors (six patients developed two tumors each, and one patient developed five independent tumors). P16 was the patient diagnosed with five PPGLs (one thoracic mediastinal paraganglioma, two periaortic, and one retrocaval abdominal paragangliomas and one pheochromocytoma; Fig. 1B). Five patients had synchronic tumors: two patients with pheochromocytoma and CB (P1 and P12); one patient with bilateral pheochromocytoma (P14); one with bilateral CB (P20); one with paraganglioma and pheochromocytoma (P26), and in two patients, the tumors were diagnosed during follow-up: one patient with pheochromocytoma and paragangliomas (P16) and the other with bilateral pheochromocytoma (P21). P18 developed a hepatic metastasis. In addition, 60 parasympathetic CBs ( $n = 24$ ; ref. 64) and head and neck ( $n = 36$ ) PPGLs developed in the context of systemic normoxia (non-CCHD) were obtained from The Central University Hospital of Asturias.

### Tumor and Germline DNA Extraction

Thirty-five of the 38 PPGL tumors (including a hepatic metastasis) from patients with CCHD were surgically excised and available for genetic analysis (Supplementary Fig. S1; Supplementary Table S1). Tumor samples were obtained in formalin-fixed, paraffin-embedded (FFPE) blocks from surgery and reviewed by a pathologist to confirm tumor type, and when the percentage of neoplastic cells was <20% in the tumor, the tumoral area was macrodissected prior to DNA extraction using the Maxwell 16 FFPE LEV DNA Purification Kit (Promega). DNA from the 60 non-CCHD CBs was previously extracted and passed internal quality control at the VHIO's laboratory before sequencing. The blood and saliva samples were collected using EDTA tubes and the Oragene OGR-500 kit (DNA Genotek), respectively, and germline DNA was extracted using Genra Puregene Blood Kit (QIAGEN). All DNA samples were quantified using a Qubit 4 Fluorometer device (Invitrogen) before downstream genetic analyses.

## Genetic Analysis

Genetic analyses on PPGL tumors from patients with CCHD and non-CCHD parasympathetic tumors were carried out using Sanger sequencing, next-generation sequencing panel, and/or WES. All patients had tumor DNA sequenced and, whenever available, their paired gDNA was also sequenced (see Supplementary Table S1 for detailed information). For Sanger sequencing, the hotspot mutation region in exon 12 of the *EPAS1* gene was analyzed by using PCR using previously described primers (40, 56): E12F-5' AACCCCCTGCTCTTTG and E12R-5' GGGGCAGATGGGGCTTAG, followed by capillary sequencing. Generated ABI files were used to assess the *EPAS1* genetic status and variant allele frequency using the Mutation Surveyor software (SoftGenetics, RRID:SCR\_001247). For WES, 1 µg of white blood cells or tumor DNA was fragmented on a hydrodynamic shearing system (Diagenode Bioruptor, RRID:SCR\_023470) to generate 180- to 280-bp fragments. The remaining overhangs were converted into blunt ends via exonuclease/polymerase activities, and enzymes were removed. After adenylation of 3'-ends of the DNA fragments, adapter oligonucleotides were ligated. DNA fragments with ligated adapter molecules on both ends were selectively enriched in PCR. Whole exomic regions were captured using the SureSelect Human All Exon V6 kit (Agilent Technologies), purified using the AMPure XP system (Beckman Coulter), and quantified using the Agilent high sensitivity DNA assay on the Agilent 2100 Bioanalyzer Instrument (Agilent Technologies, RRID:SCR\_019715). Exome sequencing was carried out on an Illumina HiSeq 4000 platform (RRID:SCR\_016386) with a median target coverage of ~200× for tumor DNA and ~100× for germline DNA. Germline and tumor WES data from 178 sympathetic PPGL tumors were retrieved from the TCGA (61, 65, 127, 128). The newly generated WES from patients with CCHD-PPGL and previously generated WES from the TCGA were processed as described below.

## WES Bioinformatics Analysis

Bioinformatics analyses were carried out by following the Genome Analysis ToolKit (GATK) Best Practices (RRID:SCR\_001876) (129) and using pipelines described in our previous genomics study; code available in <https://github.com/jfnavarro/scitron>. The FASTQ files generated from the sequencers were turned into unaligned BAM files and adaptor sequences marked to generate uBAM files, which were aligned then to the hg38 reference using the Burrows-Wheeler Aligner (BWA; RRID:SCR\_010910). Read duplicates were marked and base quality scores recalibrated. Variant calling was carried out using Mutect2 with The Genome Aggregation Database (gnomAD; RRID:SCR\_014964; ref. 130) dataset as a population resource. The variants were filtered using information about normal contamination extracted from BAM pileups at the positions of ExAc variants (RRID:SCR\_004068; ref. 131) and from a strand orientation model. The following versions of the software were used: GATK (v4.1.9.0), Samtools (1.12; RRID:SCR\_002105), and BWA (0.7.17-r).

## CN Variation, Purity, Ploidy, and Clonal Structure of *EPAS1* Mutations

For clonal structure analysis, the CN variation of the segments containing the variant was calculated using ASCAT (version 3.1.1; RRID:SCR\_016868; ref. 132) as part of the nf-core/sarek pipeline (version 3.3.2; refs. 133–135). ASCAT calculates allele-specific CN changes in a tumor sample with respect to a matched normal sample. It also estimates the purity and ploidy of the sample. CCF for *EPAS1* somatic mutations was calculated using the following formula (136):

$$\frac{VAF}{P} \cdot (P \cdot CT + (1 - P) \cdot CN)$$

where VAF is the variant allele frequency,  $P$  is the cellularity estimated from ASCAT,  $CT$  is the CN of the segment covering the position in the tumor sample, and  $CN$  is the same for the normal sample,

which is assumed to be 2 except for autosomal chromosomes. Clonal structure and phylogenetic reconstruction were performed using CONIPHER (version 2.1.0; ref. 137). Read support of autosomal single-nucleotide variants (SNV) and their associated CNs obtained from ASCAT were input to CONIPHER, setting the parameter `min_cluster_size = 2`. Clonal distribution plots were constructed using the R package cloneMap (version 1.0; bioRxiv 2022.07.26.501523) using the CCF values calculated by CONIPHER for each clone.

## Analysis of Genomic Instability in PPGL Tumors Developed under Systemic Hypoxia or Normoxia

WES data from nine *EPAS1*-mutated sympathetic PPGL tumors were generated in this study. WES data from 161 sympathetic PPGL tumors from patients without CCHD were obtained from Calsina and colleagues (85). Briefly, the FASTQ sequencing files were aligned to the human reference genome GRCh37 using the BWA (RRID:SCR\_010910; ref. 138). The Genome Analysis Toolkit GATK (139), HaplotypeCaller (bioRxiv 10.1101/201178), and MuTect (RRID:SCR\_000559; ref. 140) were used to detect SNVs and INDELS, and variant annotation was performed using the Ensembl Variant Effect Predictor tool v90 (RRID:SCR\_007931; ref. 141). SNV and INDELS were then manually curated as described in Calsina and colleagues (85) to establish the TMB of each tumor. MSI was assessed using Mantis (RRID:SCR\_021001; ref. 142). Paired normal-tumor BAM files were aligned and processed, enabling the determination of microsatellite distribution discrepancies at the somatic level. Somatic CN detection was performed with FACETS (143). The total count of CN segments, defined as somatic CN alteration burden, was computed for each sample. Details on the bioinformatic analysis of genomic instability can be obtained in Calsina and colleagues (85).

## Analysis of Frequency of *EPAS1* Somatic Mutations across Human Tumor Types (Non-PPGL)

We interrogated the *EPAS1* somatic mutation status in genomic data of 10,967 tumor samples from 32 different studies available through the PanCancer Atlas Studies of The Cancer Genome Atlas (TCGA; RRID:SCR\_003193) and 212 studies available on the cBioPortal platform (RRID:SCR\_021001; refs. 65, 127, 128). Considering previous functional studies on *EPAS1* genetic variants (40, 48), only those occurring within the oxygen-dependent degradation domain of HIF2α (amino acid residues from 528 to 542) were considered to be activating. The *EPAS1* status of the nearly 11,000 human tumors analyzed is provided in Supplementary Table S6.

## Selection Inference of *EPAS1* Mutations across Human Tumors considering Normoxia or Hypoxia Conditions

To characterize specificity of *EPAS1* mutations according to the tumor type and hypoxia condition, we inferred positive selection of these mutations on the WES data generated for CCHD-PPGL tumors and more than 10,000 tumors from 33 tumor types in the TCGA collection. Somatic mutation calls for primary tumors from TCGA were downloaded from the MC3 database (144). We inferred selection on protein-coding genes with the Cancer Bayesian Selection Estimation tool (145) separately for three cohorts: (i) 184 PPGLs from TCGA (putative non-CCHD-PPGLs; ref. 61), (ii) 10,106 TCGA tumors from 32 studies from non-PPGL tumor types, and (iii) 14 tumors from patients with CCHD-PPGL from this study. Since the CCHD-PPGL tumor samples were stored in FFPE, we manually filtered and curated the mutations as previously reported (85), leaving a total of 341 short insertions and deletions, out of which 301 were coding SNVs (i.e., missense, nonsense, or synonymous variants). *EPAS1* gene had eight missense mutations in the PPGL tumors from TCGA and seven in the CCHD-PPGL cohort.  $q$  values of mutations and mapped dN/dS are provided in Supplementary Table S2.

### Analysis of Frequency of *EPAS1* Genetic Variants in Low- and High-Altitude Natural Populations

The frequency of *EPAS1* genetic variants in 13 low-altitude populations ( $N = 148,162$  individuals) and 10 high-altitude populations ( $N = 627$  individuals) was retrieved from published data and integrated into Supplementary Table S6. High-altitude populations consisted of eight populations living across The Himalayas (Sherpas, Tibetan highlanders, Thakali, Bumthang, Chali, Brokkat, Kurtöp, and Layap) and two populations from the Andes Mountain range in South America (Colla Andean from Argentina and Quechua Peruvian highlanders from Peru). These high-altitude populations live in altitudes varying from 3,000 m to 4,450 m (average 3,749 m of altitude) on an atmospheric pressure as low as 60% of the sea level value. As a reference, the atmospheric pressure at the summit of the Everest (8,849 m) is at 30% of the sea level value. The frequency of *EPAS1* genetic variants in populations of nonhuman mammals such as horse, pig, wolf, dog, and duck living at high altitudes and of their low-altitude counterpart populations was also obtained from previous publications and integrated in Supplementary Table S6.

Nearly all *EPAS1* genetic variants found enriched at high altitudes occur in noncoding 5'-regions of the gene, mostly at the gene promoter and enhancers of the gene, and are provided in Supplementary Table S6. The frequency of these *EPAS1* noncoding genetic variants was investigated in low-altitude populations closely related to the high-altitude populations (i.e., the Han population, which is the closest related population to the highlander Tibetans), as well as in 100s of 1,000s of individuals from various low-altitude populations available through The Genome Aggregation Database (gnomAD) version 4, which is composed of 76,215 genomes from populations worldwide (130). The frequencies of these populations can be found in Supplementary Table S7. Due to the large number of populations analyzed, Fig. 1D depicts the frequencies of *EPAS1* genetic variants in some of the low- and high-altitude populations, whereas full data can be accessed in Supplementary Table S6.

### Searching for Downstream Targets of *EPAS1* Involved in Hypoxia Adaptation

As the protein encoded by *EPAS1* gene, HIF2 $\alpha$ , is a transcription factor known to control the expression of 100s of different genes, we explored RNA-seq datasets to search for downstream targets potentially involved in the observed positive selection of the *EPAS1*-mutated clones. Briefly, we used the DESeq2 package (v.1.28.1; RRID:SCR\_015687; ref. 146) to determine differentially expressed genes in *EPAS1*<sup>MUT</sup> compared with *EPAS1*<sup>WT</sup> tumors in two independent PPGL datasets, one from the TCGA (61) and the other from patients with hypoxia-associated hemoglobin disorders (59). We also searched for differentially expressed genes in PPGL-derived PC12 cell line that we cultivated in different periods of short (12, 24, and 48 hours) or prolonged (36 days, approximately 860 hours) in normoxia conditions (37°C, 5% CO<sub>2</sub>, and 21% O<sub>2</sub>) and hypoxia conditions (37°C, 5% CO<sub>2</sub>, and 1% O<sub>2</sub> balanced with N<sub>2</sub>). Detailed information about the culture conditions of the PC12 cells is shown in the Methods section called "PPGL-derived PC12 cell lines cultivated in various normoxia and hypoxia conditions."

### Measurements of DNA Repair Protein Levels in the PPGL Tumors

IHC was performed on an automatic Roche Ventana BenchMark Ultra IHC/ISH System (Roche, RRID:SCR\_025506) using 4- $\mu$ m sections of tumor FFPE blocks. Samples were stained using hematoxylin and eosin, with the specific positive control to neuroendocrine tumors (Chromogranin A, clone LK2H10) and four markers to MSI (MLH1, clone M1, Ventana Medical Systems, Cat. # 790-4535,

RRID:AB\_2336022; MSH2, clone G219-1129, Ventana Medical Systems, Cat. # 760-4265, RRID:AB\_2336002; MSH6, clone SP93, Ventana Medical Systems, Cat. # 790-4455, RRID:AB\_2336020; and PMS2, clone A16-4, Ventana Medical Systems, Cat. # 760-4531, RRID:AB\_2336010). After deparaffinization of the sections, antigen retrieval was performed using ULTRACC1 antigen retrieval buffer (6414575001, Roche) for 64 minutes at 100°C (anti-MLH1 and anti-PMS2) or for 40 minutes at 100°C (anti-MSH2 and anti-MSH6), incubation with primary antibody at 36°C (52, 16, 20, and 40 minutes respectively) and detection with Ventana OptiView DAB (Roche Cat. # 760-700, RRID:AB\_2833075). IHC results were scored by two pathologists from different institutions (coauthors R. Fasani and Y. Ding) for nuclear positivity for MSI marker protein in three categories: positive (staining in >10% nuclear tumor cells), focal positivity (staining in 1%–10% nuclear tumor cells) and negative (staining in <1% nuclear tumor cells). *H* score was obtained by multiplying the proportion of cells showing nucleus staining and the intensity of staining (0, no staining; 1, weak; 2, moderate; and 3, strong).

### Tricarboxylic Acid Cycle Metabolite Analysis in Human PPGL Tumors and Mouse PPGL-Derived Cell Line (148)

Metabolites derived from the tricarboxylic acid (TCA) cycle, including succinate, fumarate, and 2-hydroxyglutarate (2-HG), have been implicated in DNA repair mechanisms and oncogenesis (86). To investigate their role further, we quantified these oncometabolites in a preclinical PPGL model, as well as in genetically diverse PPGL tumors, including tumors harboring an *EPAS1* mutation. The preclinical PPGL model consists of MPC generated from a neurofibromin 1 knockout mouse model. TCA cycle metabolites were measured in MPCmCherry transfected with an empty vector as control and their counterparts overexpressing HIF2 $\alpha$  (87) using LC/MS-MS, following previously established methods (147). Additionally, TCA cycle-derived metabolite levels, also generated using LC/MS-MS, were examined in a diverse cohort of human 141 PPGL tumors from an existing dataset (148).

### Mitochondrial Respiration in Cells Expressing Mutant *EPAS1*

HEK293T cells, kindly provided by Dr. Josep Villanueva, were cultured in DMEM (Gibco, Thermo Fisher Scientific) supplemented with 10% FBS (Gibco, Thermo Fisher Scientific) and 1% of penicillin-streptomycin (Sigma-Aldrich). Stable cell lines were generated according to a previously described protocol (40). Briefly, cells were transfected using Lipofectamine 3000 Transfection Reagent (Thermo Fisher Scientific) and HIF2 $\alpha$  WT and HIF2 $\alpha$  P405A/P531A plasmids (Addgene plasmid IDs #26055 and #19006, respectively). Transfected cells were selected with 0.5 to 1.0  $\mu$ g/mL puromycin, and stable expression efficiency was confirmed by Western blotting against HIF2 $\alpha$  at different timepoints. Puromycin-resistant cells expressing the WT and mutant versions of HIF2 $\alpha$  were used for experiments for mitochondrial respiration measurements. These cells were aliquoted into frozen stocks, and all experiments were conducted using the same working stock and cell passage. Authentication of HEK293T cell line in the working stock and confirmation of no *Mycoplasma* contamination were conducted at the VHIR Genomic Core (Barcelona).

Mitochondrial oxygen consumption rates were measured using the Agilent Seahorse XF Cell Mito Stress Test Kit and Seahorse XFe96 FluxPak (Agilent Technologies, 103010-100 and 103721-100) in the Agilent Seahorse XFe96 Analyzer (Agilent Technologies, RRID:SCR\_019545) by following the manufacturer's instructions. About  $3 \times 10^4$  of HEK293T parental cells (condition 1), HEK293T stable cell line-expressing HIF2 $\alpha$  WT (condition 2), or HEK293T stable cell line-expressing HIF2 $\alpha$  P405A/P531A (condition 3) were plated on poly-D-lysine-coated plates on the day before the assay, including

three replicate culture wells per run. Analysis was performed in the Seahorse XF DMEM pH 7.4 (Agilent) supplemented with 10 mmol/L glucose (Agilent), 2 mmol/L glutamine (Gibco), and 1 mmol/L sodium pyruvate (Gibco). The cells were washed two times with assay media and incubated for 1 hour in a 37°C non-CO<sub>2</sub> incubator before starting the assay. Respiratory rates were measured in response to sequential injections of oligomycin (1.5 μmol/L), FCCP (1.2 μmol/L), and rotenone/antimycin A (0.5 μmol/L) and normalized to protein content per well using Pierce BCA Protein Assay Kit (Thermo Fisher Scientific). The assays were performed two times with homogeneous results. The Seahorse Analytics software was used for analysis.

### EPAS1 and COX4I2 Expression Profiles in Developmental and Adult Adrenal Medulla

In previous studies, knockout of *EPAS1* deregulated catecholamine homeostasis and cardiac stimulus (14), suggesting a direct effect of *EPAS1* on the embryological development of the sympathetic neural crest system and adrenal medulla, from which the PPGL tumors are derived. To characterize the expression profiles of *EPAS1* and *COX4I2*, its downstream target involved in mitochondrial respiration, during maturation of neural crest derivatives, we analyzed single-cell gene expression data of the entire neural crest lineage tree of mice embryos from the delamination to postnatal stages, including the domain of sympathoadrenal differentiation. These data were obtained from a previous article (91) in which the authors used the deep sequencing method Smart-seq2 (149) with the average of around 7,000 genes per individual cell. Clustering and trajectory analysis were performed, and gene expression plots of Fig. 4D were generated via the Pagoda App (<https://github.com/kharchenkolab/pagoda2>).

### PPGL-Derived PC12 Cell Lines Cultivated in Various Normoxia and Hypoxia Conditions

PC12 cells derived from rat PPGL, kindly provided by Lopez-Barneo's group and originally established by Greene and Tischler (150), were cultured in normoxia condition (37°C, 5% CO<sub>2</sub>, and 21% O<sub>2</sub>) in DMEM supplemented with 15% v/v heat-inactivated FBS, 100 U/mL penicillin, 200 μg/mL streptomycin, and 2 mmol/L L-glutamine (all from Gibco, Thermo Fisher Scientific). Cells were then either continued to be cultivated in the same normoxia condition or were placed in a hypoxic incubator (Heracell 150i CO<sub>2</sub> incubator, RRID:SCR\_026100) that maintained a constant hypoxic environment (37°C, 5% CO<sub>2</sub>, and 1% O<sub>2</sub> balanced with N<sub>2</sub>), for different short (12, 24, and 48 hours) or prolonged (36 days, approximately 860 hours) time. The cell culture medium was changed as needed. Although the cell passage number at the time of acquisition is unknown, the cells were consistently used from the same working stock at a fixed passage number for each experiment. PC12 cell authentication was confirmed by verifying the previously reported disruption of the *MAX* gene transcript in exon 3 (151), using RNA-seq data generated in this study, which has been deposited in public repositories (see "Data Availability" section). Additionally, the characteristic hypoxia-driven neurite outgrowth further validated the PC12 cell line phenotype (Supplementary Fig. S21A–S21C; ref. 152). PC12 working stock cells tested negative for *Mycoplasma* contamination at the start of the experiment, as confirmed by the University of Oviedo/Health Research Institute of Asturias (ISPA).

### RNA Extraction and RT-qPCR from PC12 Cells

Total RNA was isolated from PC12 cells using the mirVana miRNA Isolation Kit (Invitrogen) according to the manufacturer's instructions. About 100 ng of RNA was reverse transcribed with the Maxima First Strand cDNA Synthesis Kit (Thermo Fisher Scientific).

*ADORA2A* expression was analyzed using TaqMan PCR Master Mix (Applied Biosystems) in StepOnePlus Real-Time PCR System (RRID:SCR\_015805). Peptidylprolyl isomerase A mRNA was quantified to normalize the RNA input for relative quantification. All reactions were performed in triplicate, and relative mRNA expression levels were calculated using the 2<sup>-ΔΔCT</sup> method.

### RNA Extraction and RNA-seq from PC12 Cells

Total RNA was isolated using the RNeasy Mini Kit (QIAGEN), purity was checked using the NanoPhotometer spectrophotometer (Implen), and integrity and quantitation were assessed using the RNA 6000 Nano Kit of the 2100 Bioanalyzer system. A total of 1 μg RNA was used for sequencing libraries using NEBNext Ultra RNA Library Prep Kit for Illumina (New England Biolabs) by following the manufacturer's recommendations, and index codes were added to each sample. mRNA was purified using Poly T Oligo-attached magnetic beads. After fragmentation with divalent cations in elevated temperature in NEBNext First Strand Synthesis Reaction Buffer (5×), first- and second-strand cDNAs were synthesized using random hexamer primer and M-MuLV Reverse Transcriptase (RNase H-) and DNA polymerase I and RNase H, respectively. The remaining overhangs were converted into blunt ends via exonuclease/polymerase activities. After adenylation of 3'-ends of DNA fragments, NEBNext Adaptor with hairpin loop structure were ligated to prepare for hybridization. To select cDNA fragments of preferentially 150 to 200 bp in length, the library fragments were purified with AMPure XP system (Beckman Coulter). Then, 3 μL of USER Enzyme (New England Biolabs) was used with size-selected, adaptor-ligated cDNA at 37°C for 15 minutes followed by 5 minutes at 95°C before PCR. Then, PCR was performed with Phusion High-Fidelity DNA Polymerase, Universal PCR primers and Index Primer. PCR products were purified (AMPure XP system); library quality was assessed on the Agilent 2100 Bioanalyzer system and sequenced on Illumina NovaSeq 6000 platform (RRID:SCR\_016387).

### Analysis of Differentially Expressed Genes in PC12 Cells in Hypoxia and PPGL Tumors

For bioinformatics analysis, adapter removal and filtering of bad-quality paired-end reads was performed using the *fastp* software (v.0.11.9; ref. 153) with the options: `-detect_adapter_for_pe -trim_poly_x -correction -r -M 10 -l 20`. The subsequent filtered reads were pseudo-aligned to the *rn6* rat genome and quantified at the transcript level using *Salmon* package (v.1.3.0; ref. 154). A prior salmon indexing step was created using a genome file composed by the concatenation of the Ensembl Rnor\_6.0 transcriptome and genome assemblies. Transcript-level information was summarized to the gene level for both exploratory and differential analyses with *tximport* package (v.1.16.1; ref. 155). The matrix of raw counts was rlog-transformed for visualization purposes and normalized for differential gene expression (DEG) analyses according to the *DESeq2* package (v.1.28.1; ref. 146). Genes that were not expressed (<2 counts across all conditions) were discarded to reduce the multiple testing penalty. Likelihood ratio test analysis was performed to identify differentially expressed genes between the three main conditions selected from exploratory studies (normoxia, hypoxia, and prolonged hypoxia, 36 days). Genes with an FDR < 0.05 were considered as significant for downstream purposes. Gene coexpression analyses were performed using *degPatterns* function from the *DEGreport* package (v.1.24.1; <http://lpantano.github.io/DEGreport/>, RRID:SCR\_018941), on the rlog normalized expression matrix containing the combined significant genes detected across all comparisons in the aforementioned differential expression analyses. Over-representation analysis of the biological functions associated with each of the modules was conducted using the *goseq* package (v.1.40.0; ref. 156) using the Gene

Ontology, Kyoto Encyclopedia of Genes and Genomes, and MSigDB Hallmark gene sets (157). The gene length bias inherent to RNA-seq data was considered for these analyses. For the patient samples of PPGL, log fold changes and *q* values of genes were obtained from TCGA (61, 65, 127, 128). Differential expression analysis for the PPGL-derived cell-line samples was performed using the R package DESeq2 (version 1.40.0; ref. 146). Genes with adjusted *P* value < 0.01 were considered differentially expressed. The lfcShrink function from DESeq2 was used for visualization purposes. All gene expression data analyses were conducted using the statistical software R (v.4.0.2).

### Western Blotting

Protein extracts were obtained from PC12 cells at 80% to 90% confluence. Cells were lysed using ice-cold RIPA buffer (Sigma-Aldrich) supplemented with phosphatase-inhibitor (Sigma-Aldrich) and protease-inhibitor (Roche) cocktail. Total protein concentration was measured using Dye Reagent Concentrate (Bio-Rad) by a colorimetric assay based on the Bradford method. Equal amounts of proteins were fractionated on SDS-PAGE and transferred to polyvinylidene difluoride membranes. Membranes were probed with rabbit anti-Phospho-Histone H2A.X (Cell Signaling Technology, Cat. # 9718, RRID:AB\_2118009) at 1:500 dilution, rabbit anti-PARP1 (Abcam, Cat. # ab191217, RRID:AB\_2861274) at 1:500 dilution, rabbit anti-Caspase-3 (Cell Signaling Technology, Cat. # 14220, RRID:AB\_2798429) at 1:500 dilution, rabbit anti-HIF-2 $\alpha$  (Abcam, Cat. # ab199, RRID:AB\_302739) at 1:250 dilution, or mouse anti- $\beta$ -actin (Sigma-Aldrich, Cat. # A1978, RRID:AB\_476692) at 1:10,000 dilution. Bound antibodies were detected by using IRDye 800CW (LI-COR Biosciences, Cat. # 925-32411, RRID:AB\_2814905) or IRDye 680RD IgG secondary antibodies (LI-COR Biosciences, Cat. # 926-68071, RRID:AB\_10956166) at 1:10,000 dilution. Image acquisition and densitometric analysis were performed using the LI-COR Odyssey Fc Imaging System (RRID:SCR\_123227). Full Western blot images are presented in Supplementary Figs. S22 and S23.

### Immunofluorescence

Cells were fixed for 15 minutes in 4% paraformaldehyde and permeabilized with PBS containing 0.1% Triton X-100. Primary antibodies (rabbit anti-Phospho-Histone H2A.X at 1:250 dilution and rabbit anti-PARP1 at 1:100 dilution) were incubated overnight. Chicken anti-rabbit Alexa Fluor 488 (Molecular Probes, Cat. # A-21441, RRID:AB\_2535859) or goat anti-rabbit Alexa Fluor 555 (Thermo Fisher Scientific, Cat. # A32814TR, RRID:AB\_2866497) were used as secondary antibody at 1:500 dilution for 1 hour. EverBrite Mounting Medium with DAPI (Biotium) was added for nuclear staining. Images were taken using a Zeiss Axio Observer microscope (Carl Zeiss, RRID:SCR\_021351) with a Plan-Apochromat 40 $\times$ /1.3 (NA = 1.3, working distance = 0.21 mm) or Plan-Apochromat 63 $\times$ /1.4 (NA = 1.4, working distance = 0.19 mm) oil lens objective, a camera (AxioCam MRm; Carl Zeiss), and ApoTome (ApoTome.2; Carl Zeiss).

### Comet Assay

The alkaline comet assay was performed as described by Espina and colleagues (158). Briefly,  $1.5 \times 10^5$  PC12 cells cultured under normoxic (21% O<sub>2</sub>) or hypoxic conditions (1% O<sub>2</sub>) for 30 hours or 36 days were embedded in 0.5% low melting point agarose (Invitrogen) and immediately pipetted onto slides precoated with 0.5% normal melting point agarose. Gel-coated slides were lysed in alkaline buffer (pH 10) for 1 hour, denatured at pH 13 for 20 minutes, and subjected to electrophoresis for 20 minutes. All these steps were

carried out at 4°C in the dark. The slides were then neutralized (pH 7.5), fixed in absolute ethanol, and air-dried overnight. For visualization, each slide, coded for blind analysis, was stained with ethidium bromide and examined under a fluorescence microscope (Olympus BX61 Upright Wide Field Microscope; RRID:SCR\_020343) at 400 $\times$  magnification. Images of at least 50 comet nucleoids per slide were taken and subsequently analyzed using KOMET 5 software (Kinetic Imaging Limited, now Oxford Instruments Andor). The percentage of DNA in the comet tail (% tail DNA) was used to measure DNA damage. Two slides per condition were scored for each experiment, with three independent experiments performed.

### Belzutifan Treatment in HEK293T Stable Cell Line Expressing HIF2 $\alpha$ -WT and HIF2 $\alpha$ -P405A/P531A Mutant

About  $3 \times 10^5$  of HEK293T parental cells (EV); HEK293T cells transfected, which stably express HIF2 $\alpha$  WT; and HIF2 $\alpha$  P405A/P531A under the pressure of puromycin antibiotic were seeded in six-well plates. The cells were treated with 100  $\mu$ mol/L of belzutifan drug (HIF2 $\alpha$  inhibitor, PT2977, MedChemExpress), whereas DMSO was used as a control. A time-course analysis to assess cell proliferation was performed at 24, 48, and 72 hours. After the specified treatment durations, cells were detached and counted using Beckman Coulter Vi-CELL XR Cell Viability Analyzer (Beckman Coulter Life Sciences, RRID:SCR\_019664). The drug concentration was previously estimated by testing different concentrations using CellTiter-Blue Cell Viability Assay (Promega).

### Data Availability

The clinical data of the patients included in the study (N=2,854), and the frequencies of *EPAS1* variants in natural populations (N=148,789) and in cancer cohorts (N=11,297) are available in supplementary tables (Supplementary Tables S1-S8, S12-S16) for purposes of reproducing or extending the analysis. Newly generated whole-exome sequencing and RNA-seq data (Supplementary Tables S1, S11) supporting the findings of this study have been deposited in the European Genome Phenome Archive (EGA) under the study ID EGAC5000000484 and dataset IDs EGAD50000001200 and EGAD50000001201. These datasets are available under controlled access with appropriate Data Use Ontology (DUO) codes (DUO: 0000020, DUO: 0000021, DUO: 0000025, DUO: 0000006). Further details about EGA are available at <https://ega-archive.org> and in the publication “The European Genome-phenome Archive in 2021” (<https://academic.oup.com/nar/advance-article/doi/10.1093/nar/gkab1059/6430505>). Variant call format (VCF) files containing somatic mutations identified in PPGL tumors through paired germline:tumor WES are deposited in the Zenodo repository and are accessible upon authorized permission at <https://zenodo.org/records/14960664>. Additionally, RNA-Seq data from PPGL-derived PC12 cell lines cultured under normoxia and hypoxia conditions have been deposited in the Sequence Read Archive (SRA) under accession number PRJNA1221786, available at <https://www.ncbi.nlm.nih.gov/sra>.

### Authors' Disclosures

C. Arenillas reports grants from the CIBERONC Spanish Network during the conduct of the study. J.J. Alba-Linares reports grants from the Spanish Association Against Cancer (AECC) during the conduct of the study. T. Dwight reports grants from the National Health and Medical Research Council (Australia; APP1108032) and Hillcrest Foundation (Perpetual IMPACT Philanthropy Program) during the conduct of the study. R. Clifton-Bligh reports personal fees from Kyowa Kirin, Lilly, Specialized Therapeutics, and the Endocrine Society

outside the submitted work. R. Dienstmann reports personal fees from Roche, Foundation Medicine, Guardant Health, Ipsen, Amgen, Servier, Sanofi, Libbs Farmacéutica, Merck Sharp & Dohme, Eli Lilly, Johnson & Johnson, Bristol Myers Squibb, Gilead Sciences, Takeda, and Daiichi Sankyo; grants and personal fees from AstraZeneca, Merck, GlaxoSmithKline, Pfizer, and Novartis outside the submitted work; as well as investing in Trialing Health S.L. J. Capdevila reports grants and personal fees from Exelixis, Roche, Ipsen, Novartis, Eisai, and ITM; personal fees from Merck, Lilly, and Esteve during the conduct of the study; as well as grants from AstraZeneca and Gilead. J. Favier reports grants from Ligue contre le Cancer, the Association Surrénales, and the Institut National du Cancer during the conduct of the study. P. Nuciforo reports personal fees from Discovery Life Sciences outside the submitted work. N. Bechmann reports grants from the German Research Foundation during the conduct of the study. P.L.M. Dahia reports grants from the NIH/NIGMS, NIH/NCI, NCTRF, VHL Alliance, and Paradifference Foundation outside the submitted work; as well as other support from holding the Robert Tucker Hayes Distinguished Chair in Oncology during the conduct of the study. R.A. Toledo reports grants from the Paradifference Foundation, the Pheipas Patients Association, the Foundation for Oncological Studies and Research (FERO), the Banco Bilbao Vizcaya Argentaria (BBVA) Foundation, AstraZeneca, BeiGene Pharmaceuticals, Novartis, La Caixa Foundation, and the Agency for Management of University and Research Grants (AGAUR) outside the submitted work; grants and personal fees from the Institute of Health Carlos III (ISCIII) of the Ministry of Economy and Competitiveness from the Spanish government; nonfinancial support from the European Network for the Study of Adrenal Tumors (ENS@T); other support from COST Action CA20122 Harmonisation, the State Research Agency (Agencia Estatal de Investigación), the Cellex Foundation, the CERCA Programme from the Generalitat de Catalunya, and other support from Personalis, Inc.; as well as, nonfinancial support from the CIBERONC Spanish Network during the conduct of the study. No disclosures were reported by the other authors.

## Authors' Contributions

**C. Arenillas:** Resources, data curation, formal analysis, supervision, investigation, visualization, methodology, writing–review and editing. **L. Celada:** Data curation, formal analysis, investigation, visualization, methodology. **J. Ruiz-Cantador:** Resources, methodology. **B. Calsina:** Data curation, formal analysis, investigation, visualization, methodology, writing–review and editing. **D. Data:** Data curation, software, formal analysis, investigation, visualization, methodology. **E. García-Galea:** Data curation, software, formal analysis, investigation, visualization, methodology. **R. Fasani:** Data curation, formal analysis, investigation, visualization, methodology. **A.B. Moreno-Cárdenas:** Investigation, methodology. **J.J. Alba-Linares:** Data curation, software, formal analysis, investigation, methodology. **B. Miranda-Barrio:** Resources, data curation, formal analysis, investigation, methodology. **A.M. Martínez-Montes:** Data curation, software, investigation, methodology. **C. Alvarez-Escola:** Resources. **B. Lecumberri:** Resources. **A. González García:** Resources. **S. K. Flores:** Investigation, methodology. **E. Esquivel:** Investigation, methodology. **Y. Ding:** Data curation, formal analysis, investigation, methodology. **M. Peitzsch:** Investigation, methodology. **J.A. Robles-Guirado:** Formal analysis, investigation, visualization, methodology. **R.M. Regojo Zapata:** Resources. **J.J. Pozo-Kreilinger:** Resources. **C. Iglesias:** Resources, formal analysis. **T. Dwight:** Investigation, methodology. **C.A. Muir:** Resources, methodology, writing–review and editing. **A. Oleaga:** Resources. **M.E. Garrido-Lestache Rodríguez-Monte:** Resources. **M.J. Del Cerro:** Resources. **I. Martínez-Bendayán:** Resources. **E. Álvarez-González:** Investigation, methodology. **T. Cubiella:**

Investigation, methodology. **D.M. Lourenço Jr:** Resources. **M.A. A. Pereira:** Resources. **N. Burnichon:** Resources, investigation. **A. Buffet:** Resources, investigation. **C. Broberg:** Resources. **P.V. Dickson:** Resources. **M.F. Fraga:** Software. **J.L. Llorente Pendás:** Resources. **J. Rueda Soriano:** Resources. **F. Buendía Fuentes:** Resources. **S.P.A. Toledo:** Investigation, methodology. **R. Clifton-Bligh:** Resources. **R. Dienstmann:** Software. **J. Villanueva:** Resources, methodology. **J. Capdevila:** Resources. **A.-P. Gimenez-Roqueplo:** Resources, investigation. **J. Favier:** Resources, investigation. **P. Nuciforo:** Resources, investigation. **W.F. Young Jr:** Resources. **N. Bechmann:** Resources, data curation, formal analysis, investigation, methodology. **A.R. Opatowsky:** Resources, methodology, writing–review and editing. **A. Vaidya:** Resources, data curation, methodology. **I. Bancos:** Resources, data curation. **D. Weghorn:** Data curation, software, formal analysis, investigation, visualization, methodology, writing–review and editing. **M. Robledo:** Resources, formal analysis, investigation, methodology. **A. Casteràs:** Resources, data curation, investigation, methodology. **L. Dos-Subirà:** Resources, data curation, investigation, methodology. **I. Adameyko:** Resources, data curation, software, formal analysis, investigation, visualization, methodology, writing–review and editing. **M.-D. Chiara:** Resources, data curation, formal analysis, investigation, visualization, methodology. **P.L.M. Dahia:** Resources, data curation, formal analysis, supervision, investigation, visualization, methodology, writing–review and editing. **R.A. Toledo:** Conceptualization, resources, data curation, formal analysis, supervision, funding acquisition, investigation, visualization, methodology, writing–original draft, project administration, writing–review and editing.

## Acknowledgments

The authors would like to thank especially patients and their families for their participation and contribution to this research study. We acknowledge IdiPAZ Biobank for the assistance in some tumor samples collection; VHIO's Oncology Data Science (ODysSey) for carrying out some statistical analyses; European Network for the Study of Adrenal Tumors (ENS@T) and COST Action CA20122 Harmonisation for supportive networking; FERO Foundation for providing a startup grant for VHIO's Biomarkers and Clonal Dynamics Laboratory led by R.A. Toledo; and Editage for its editing services. VHIO would like to acknowledge: the State Agency for Research (Agencia Estatal de Investigación) for the financial support as a Center of Excellence Severo Ochoa (CEX2020-001024-S/AEI/10.13039/501100011033), the Cellex Foundation for providing research facilities and equipment, the CERCA Programme from the Generalitat de Catalunya for their support on this research, and the Banco Bilbao Vizcaya Argentaria (BBVA) Foundation for supporting the Comprehensive Program of Cancer Immunotherapy and Immunology (CAIMI-I and CAIMI-II, grant no. 53/2021). In memory of Dr. José María Oliver, who played a pivotal role in the development of the field of Adult Congenital Heart Diseases in Spain and his early assessment of CCHD and PPGL association. The sponsors of this study listed below supported the costs related to the research experiments and salary of the investigators. Paradifference Foundation supported this PPGL research and provided funding support to J. Favier, M. Robledo, I. Adameyko, P.L.M. Dahia, and R.A. Toledo. The Pheipas Patient Association provided a research grant to R.A. Toledo for the study of PPGL tumors (grant #914300). C. Arenillas was supported by a CIBERONC predoctoral fellowship. R.A. Toledo holds a Miguel Servet-I research contract and a Plan Nacional grant by the Institute of Health Carlos III (ISCIII) of the Ministry of Economy and Competitiveness from the Spanish government (grants #CP17/00199 and #PID2021-126297OA-I00). P.L.M. Dahia received grants from the NIH/NIGMS (#GM114102), NIH/NCI (#CA264248), Neuroendocrine Tumor Research Foundation (NETRF), VHL Alliance, Paradifference Foundation and is

the holder of the Robert Tucker Hayes Distinguished Chair in Oncology. M.-D. Chiara received grants from the Institute of Health Carlos III (ISCIII) of the Ministry of Economy and Competitiveness from the Spanish government (grants #PI20/01754 and #PID2023-151388OB-I00). J. Capdevila was partially supported by the Institute of Health Carlos III (ISCIII; #PI20/00895) and co-funded by the European Union (ERDF/ESF)—A way to build Europe and the Enric Masip Foundation. C. Arenillas, B. Calsina, T. Cubiella, J. Favier, M. Robledo, M.-D. Chiara, and R.A. Toledo were awarded with travel grants by European Cooperation in Science and Technology (COST) Action CA20122 Harmonisation.

## Note

Supplementary data for this article are available at Cancer Discovery Online (<http://cancerdiscovery.aacrjournals.org/>).

Received July 4, 2024; revised November 21, 2024; accepted January 27, 2025; published first April 8, 2025.

## REFERENCES

- Luo G, Ono S, Beukes NJ, Wang DT, Xie S, Summons RE. Rapid oxygenation of Earth's atmosphere 2.33 billion years ago. *Sci Adv* 2016;2:e1600134.
- Gray MW. Mitochondrial evolution. *Cold Spring Harb Perspect Biol* 2012;4:a011403.
- Chandel NS. Evolution of mitochondria as signaling organelles. *Cell Metab* 2015;22:204–6.
- Martínez-Reyes I, Chandel NS. Mitochondrial TCA cycle metabolites control physiology and disease. *Nat Commun* 2020;11:102.
- Semenza GL. HIF-1, O<sub>2</sub>, and the 3 PHDs: how animal cells signal hypoxia to the nucleus. *Cell* 2001;107:1–3.
- Wang GL, Jiang BH, Rue EA, Semenza GL. Hypoxia-inducible factor 1 is a basic-helix-loop-helix-PAS heterodimer regulated by cellular O<sub>2</sub> tension. *Proc Natl Acad Sci U S A* 1995;92:5510–4.
- Maxwell PH, Wiesener MS, Chang GW, Clifford SC, Vaux EC, Cockman ME, et al. The tumour suppressor protein VHL targets hypoxia-inducible factors for oxygen-dependent proteolysis. *Nature* 1999;399:271–5.
- Ohh M, Park CW, Ivan M, Hoffman MA, Kim TY, Huang LE, et al. Ubiquitination of hypoxia-inducible factor requires direct binding to the beta-domain of the von Hippel-Lindau protein. *Nat Cell Biol* 2000;2:423–7.
- Jaakkola P, Mole DR, Tian YM, Wilson MI, Gielbert J, Gaskell SJ, et al. Targeting of HIF- $\alpha$  to the von Hippel-Lindau ubiquitylation complex by O<sub>2</sub>-regulated prolyl hydroxylation. *Science* 2001;292:468–72.
- Ivan M, Kondo K, Yang H, Kim W, Valiano J, Ohh M, et al. HIF $\alpha$  targeted for VHL-mediated destruction by proline hydroxylation: implications for O<sub>2</sub> sensing. *Science* 2001;292:464–8.
- Flamme I, Fröhlich T, Von Reutern M, Kappel A, Damert A, Risau W. HRF, a putative basic helix-loop-helix-PAS-domain transcription factor is closely related to hypoxia-inducible factor-1  $\alpha$  and developmentally expressed in blood vessels. *Mech Dev* 1997;63:51–60.
- Tian H, McKnight SL, Russell DW. Endothelial PAS domain protein 1 (EPAS1), a transcription factor selectively expressed in endothelial cells. *Genes Dev* 1997;11:72–82.
- Ema M, Taya S, Yokotani N, Sogawa K, Matsuda Y, Fujii-Kuriyama Y. A novel bHLH-PAS factor with close sequence similarity to hypoxia-inducible factor 1 $\alpha$  regulates the VEGF expression and is potentially involved in lung and vascular development. *Proc Natl Acad Sci U S A* 1997;94:4273–8.
- Tian H, Hammer RE, Matsumoto AM, Russell DW, McKnight SL. The hypoxia-responsive transcription factor EPAS1 is essential for catecholamine homeostasis and protection against heart failure during embryonic development. *Genes Dev* 1998;12:3320–4.
- López-Barneo J, López-López JR, Ureña J, González C. Chemotransduction in the carotid body: K<sup>+</sup> current modulated by PO<sub>2</sub> in type I chemoreceptor cells. *Science* 1988;241:580–2.
- Moreno-Domínguez A, Ortega-Sáenz P, Gao L, Colinas O, García-Flores P, Bonilla-Henao V, et al. Acute O<sub>2</sub> sensing through HIF2 $\alpha$ -dependent expression of atypical cytochrome oxidase subunits in arterial chemoreceptors. *Sci Signal* 2020;13:eaay9452.
- Comline RS, Silver M. The development of the adrenal medulla of the foetal and new-born calf. *J Physiol* 1966;183:305–40.
- Seidler FJ, Slotkin TA. Adrenomedullary function in the neonatal rat: responses to acute hypoxia. *J Physiol* 1985;358:1–16.
- Tissot Van Patot MC, Gassmann M. Hypoxia: adapting to high altitude by mutating EPAS-1, the gene encoding HIF-2 $\alpha$ . *High Alt Med Biol* 2011;12:157–67.
- Semenza GL, Neifelt MK, Chi SM, Antonarakis SE. Hypoxia-inducible nuclear factors bind to an enhancer element located 3' to the human erythropoietin gene. *Proc Natl Acad Sci U S A* 1991;88:5680–4.
- Pugh CW, Tan CC, Jones RW, Ratcliffe PJ. Functional analysis of an oxygen-regulated transcriptional enhancer lying 3' to the mouse erythropoietin gene. *Proc Natl Acad Sci U S A* 1991;88:10553–7.
- Yi X, Liang Y, Huerta-Sanchez E, Jin X, Cuo ZXP, Pool JE, et al. Sequencing of 50 human exomes reveals adaptation to high altitude. *Science* 2010;329:75–8.
- Simonson TS, Yang Y, Huff CD, Yun H, Qin G, Witherspoon DJ, et al. Genetic evidence for high-altitude adaptation in Tibet. *Science* 2010;329:72–5.
- Bigham A, Bauchet M, Pinto D, Mao X, Akey JM, Mei R, et al. Identifying signatures of natural selection in Tibetan and Andean populations using dense genome scan data. *PLoS Genet* 2010;6:e1001116.
- Beall CM, Cavalleri GL, Deng L, Elston RC, Gao Y, Knight J, et al. Natural selection on EPAS1 (HIF2 $\alpha$ ) associated with low hemoglobin concentration in Tibetan highlanders. *Proc Natl Acad Sci U S A* 2010;107:11459–64.
- Liu X, Zhang Y, Li Y, Pan J, Wang D, Chen W, et al. EPAS1 gain-of-function mutation contributes to high-altitude adaptation in Tibetan horses. *Mol Biol Evol* 2019;36:2591–603.
- Gou X, Wang Z, Li N, Qiu F, Xu Z, Yan D, et al. Whole-genome sequencing of six dog breeds from continuous altitudes reveals adaptation to high-altitude hypoxia. *Genome Res* 2014;24:1308–15.
- Zhang W, Fan Z, Han E, Hou R, Zhang L, Galaverni M, et al. Hypoxia adaptations in the grey wolf (*Canis lupus chanco*) from Qinghai-Tibet Plateau. *PLoS Genet* 2014;10:e1004466.
- Ma YF, Han XM, Huang CP, Zhong L, Adeola AC, Irwin DM, et al. Population genomics analysis revealed origin and high-altitude adaptation of Tibetan pigs. *Sci Rep* 2019;9:11463.
- Graham AM, McCracken KG. Convergent evolution on the hypoxia-inducible factor (HIF) pathway genes EGLN1 and EPAS1 in high-altitude ducks. *Heredity (Edinb)* 2019;122:819–32.
- Peng Y, Cui C, He Y, Ouzhuluobu, Zhang H, Yang D, et al. Down-regulation of EPAS1 transcription and genetic adaptation of Tibetans to high-altitude hypoxia. *Mol Biol Evol* 2017;34:818–30.
- Gray OA, Yoo J, Sobreira DR, Jousma J, Witonsky D, Sakabe NJ, et al. A pleiotropic hypoxia-sensitive EPAS1 enhancer is disrupted by adaptive alleles in Tibetans. *Sci Adv* 2022;8:eade1942.
- Xin J, Zhang H, He Y, Duren Z, Bai C, Chen L, et al. Chromatin accessibility landscape and regulatory network of high-altitude hypoxia adaptation. *Nat Commun* 2020;11:4928.
- Jorgensen K, Song D, Weinstein J, García OA, Pearson LN, Inclán M, et al. High-altitude andean H194R HIF2A allele is a hypomorphic allele. *Mol Biol Evol* 2023;40:msad162.
- Storz JF, Signore A V. Introgressive hybridization and hypoxia adaptation in high-altitude vertebrates. *Front Genet* 2021;12:696484.
- Huerta-Sánchez E, Jin X, Asan, Bianba Z, Peter BM, Vinckenbosch N, et al. Altitude adaptation in Tibetans caused by introgression of Denisovan-like DNA. *Nature* 2014;512:194–7.
- Hu H, Petousi N, Glusman G, Yu Y, Bohlender R, Tashi T, et al. Evolutionary history of Tibetans inferred from whole-genome sequencing. *PLoS Genet* 2017;13:e1006675.

38. Zhang X, Witt KE, Bañuelos MM, Ko A, Yuan K, Xu S, et al. The history and evolution of the Denisovan-EPAS1 haplotype in Tibetans. *Proc Natl Acad Sci U S A* 2021;118:e2020803118.
39. Patel SA, Simon MC. Biology of hypoxia-inducible factor-2alpha in development and disease. *Cell Death Differ* 2008;15:628–34.
40. Toledo RA, Qin Y, Srikanth S, Morales NP, Li Q, Deng Y, et al. In vivo and in vitro oncogenic effects of HIF2A mutations in pheochromocytomas and paragangliomas. *Endocr Relat Cancer* 2013;20:349–59.
41. Kondo K, Kim WY, Lechpammer M, Kaelin WG. Inhibition of HIF2alpha is sufficient to suppress pVHL-defective tumor growth. *PLoS Biol* 2003;1:E83.
42. Choueiri TK, Bauer TM, Papadopoulos KP, Plimack ER, Merchan JR, McDermott DF, et al. Inhibition of hypoxia-inducible factor-2α in renal cell carcinoma with belzutifan: a phase 1 trial and biomarker analysis. *Nat Med* 2021;27:802–5.
43. Jonasch E, Donskov F, Iliopoulos O, Rathmell WK, Narayan VK, Maughan BL, et al. Belzutifan for renal cell carcinoma in von Hippel-Lindau disease. *N Engl J Med* 2021;385:2036–46.
44. Toledo RA, Jimenez C, Armaiz-Pena G, Arenillas C, Capdevila J, Dahia PLM. Hypoxia-inducible factor 2 alpha (HIF2α) inhibitors: targeting genetically driven tumor hypoxia. *Endocr Rev* 2023;44:312–22.
45. Cho H, Du X, Rizzi JP, Liberzon E, Chakraborty AA, Gao W, et al. On-target efficacy of a HIF-2α antagonist in preclinical kidney cancer models. *Nature* 2016;539:107–11.
46. Choueiri TK, Kaelin WG. Targeting the HIF2-VEGF axis in renal cell carcinoma. *Nat Med* 2020;26:1519–30.
47. Comino-Méndez I, de Cubas AA, Bernal C, Álvarez-Escolá C, Sánchez-Malo C, Ramírez-Tortosa CL, et al. Tumoral EPAS1 (HIF2A) mutations explain sporadic pheochromocytoma and paraganglioma in the absence of erythrocytosis. *Hum Mol Genet* 2013;22:2169–76.
48. Zhuang Z, Yang C, Lorenzo F, Merino M, Fojo T, Kebebew E, et al. Somatic HIF2A gain-of-function mutations in paraganglioma with polycythemia. *N Engl J Med* 2012;367:922–30.
49. NGS in PPGL NGSnPPGL Study Group; Toledo RA, Burnichon N, Cascon A, Benn DE, Bayley JP, et al. Consensus Statement on next-generation-sequencing-based diagnostic testing of hereditary pheochromocytomas and paragangliomas. *Nat Rev Endocrinol* 2017;13:233–47.
50. Dahia PLM. Pheochromocytoma and paraganglioma pathogenesis: learning from genetic heterogeneity. *Nat Rev Cancer* 2014;14:108–19.
51. Arias-Stella J, Valcarcel J. Chief cell hyperplasia in the human carotid body at high altitudes; physiologic and pathologic significance. *Hum Pathol* 1976;7:361–73.
52. Arias-Stella J, Valcarcel J. The human carotid body at high altitudes. *Pathol Microbiol (Basel)* 1973;39:292–7.
53. Saldana MJ, Salem LE, Travezan R. High altitude hypoxia and chemodectomas. *Hum Pathol* 1973;4:251–63.
54. Opatowsky AR, Moko LE, Ginns J, Rosenbaum M, Greutmann M, Aboulhosn J, et al. Pheochromocytoma and paraganglioma in cyanotic congenital heart disease. *J Clin Endocrinol Metab* 2015;100:1325–34.
55. Ponz de Antonio I, Ruiz Cantador J, González García AE, Oliver Ruiz JM, Sánchez-Recalde Á, López-Sendón JL. Prevalence of neuroendocrine tumors in patients with cyanotic congenital heart disease. *Rev Esp Cardiol (Engl Ed)* 2017;70:673–5.
56. Vaidya A, Flores SK, Cheng Z-M, Nicolas M, Deng Y, Opatowsky AR, et al. EPAS1 mutations and paragangliomas in cyanotic congenital heart disease. *N Engl J Med* 2018;378:1259–61.
57. Ogasawara T, Fujii Y, Kakiuchi N, Shiozawa Y, Sakamoto R, Ogawa Y, et al. Genetic analysis of pheochromocytoma and paraganglioma complicating cyanotic congenital heart disease. *J Clin Endocrinol Metab* 2022;107:2545–55.
58. White G, Nonaka D, Chung T-T, Oakey RJ, Izatt L. Somatic EPAS1 variants in pheochromocytoma and paraganglioma in patients with sickle cell disease. *J Clin Endocrinol Metab* 2023;108:3302–10.
59. Mancini M, Buffet A, Porte B, Amar L, Lussey-Lepoutre C, Crinière L, et al. EPAS1-mutated paragangliomas associated with haemoglobin disorders. *Br J Haematol* 2024;204:1054–60.
60. Huang LE, Gu J, Schau M, Bunn HF. Regulation of hypoxia-inducible factor 1alpha is mediated by an O<sub>2</sub>-dependent degradation domain via the ubiquitin-proteasome pathway. *Proc Natl Acad Sci U S A* 1998;95:7987–92.
61. Fishbein L, Leshchiner I, Walter V, Danilova L, Robertson AG, Johnson AR, et al. Comprehensive molecular characterization of pheochromocytoma and paraganglioma. *Cancer Cell* 2017;31:181–93.
62. McGranahan N, Favero F, De Bruin EC, Birkbak NJ, Szallasi Z, Swanton C. Clonal status of actionable driver events and the timing of mutational processes in cancer evolution. *Sci Transl Med* 2015;7:283ra54.
63. Snezhkina AV, Lukyanova EN, Kalinin DV, Pokrovsky AV, Dmitriev AA, Koroban NV, et al. Exome analysis of carotid body tumor. *BMC Med Genomics* 2018;11:17.
64. Bernardo-Castiñeira C, Sáenz-de-Santa-María I, Valdés N, Astudillo A, Balbín M, Pitiot AS, et al. Clinical significance and peculiarities of succinate dehydrogenase B and hypoxia inducible factor 1α expression in parasympathetic versus sympathetic paragangliomas. *Head Neck* 2019;41:79–91.
65. Gao J, Aksoy BA, Dogrusoz U, Dresdner G, Gross B, Sumer SO, et al. Integrative analysis of complex cancer genomics and clinical profiles using the cBioPortal. *Sci Signal* 2013;6:pl1.
66. Cancer Genome Atlas Research Network; Weinstein JN, Collisson EA, Mills GB, Shaw KRM, Ozenberger BA, et al. The Cancer Genome Atlas pan-cancer analysis project. *Nat Genet* 2013;45:1113–20.
67. Zhang XL, Ha BB, Wang SJ, Chen ZJ, Ge JY, Long H, et al. The earliest human occupation of the high-altitude Tibetan plateau 40 thousand to 30 thousand years ago. *Science* 2018;362:1049–51.
68. Zhang D, Xia H, Chen F, Li B, Slon V, Cheng T, et al. Denisovan DNA in late pleistocene sediments from baishiya karst cave on the Tibetan plateau. *Science* 2020;370:584–7.
69. Zhang JF, Dennell R. The last of Asia conquered by Homo sapiens. *Science* 2018;362:992–3.
70. Villafuerte FC, Cárdenas R, Monge-C C. Optimal hemoglobin concentration and high altitude: a theoretical approach for Andean men at rest. *J Appl Physiol* 1985 2004;96:1581–8.
71. Beall CM. Two routes to functional adaptation: Tibetan and Andean high-altitude natives. *Proc Natl Acad Sci U S A* 2007;104(Suppl 1):8655–60.
72. Eichstaedt CA, Pagani L, Antao T, Inchley CE, Cardona A, Mörseburg A, et al. Evidence of early-stage selection on EPAS1 and GPR126 genes in andean high altitude populations. *Sci Rep* 2017;7:13042.
73. Bhandari S, Zhang X, Cui C, Yangla Liu L, Liu L, Ouzhuluobu, et al. Sherpas share genetic variations with Tibetans for high-altitude adaptation. *Mol Genet Genomic Med* 2016;5:76–84.
74. Jeong C, Alkorta-Aranburu G, Basnyat B, Neupane M, Witonsky DB, Pritchard JK, et al. Admixture facilitates genetic adaptations to high altitude in Tibet. *Nat Commun* 2014;5:3281.
75. Lawrence ES, Gu W, Bohlender RJ, Anza-Ramirez C, Cole AM, Yu JJ, et al. Functional EPAS1/HIF2A missense variant is associated with hematocrit in Andean highlanders. *Sci Adv* 2024;10:5661.
76. Reich D, Green RE, Kircher M, Krause J, Patterson N, Durand EY, et al. Genetic history of an archaic hominin group from Denisova Cave in Siberia. *Nature* 2010;468:1053–60.
77. Bhandari V, Hoey C, Liu LY, Lalonde E, Ray J, Livingstone J, et al. Molecular landmarks of tumor hypoxia across cancer types. *Nat Genet* 2019;51:308–18.
78. Bhandari V, Li CH, Bristow RG, Boutros PC; PCAWG Consortium. Divergent mutational processes distinguish hypoxic and normoxic tumours. *Nat Commun* 2020;11:737.
79. Yuan J, Glazer PM. Mutagenesis induced by the tumor microenvironment. *Mutat Res* 1998;400:439–46.

80. Mihaylova VT, Bindra RS, Yuan J, Campisi D, Narayanan L, Jensen R, et al. Decreased expression of the DNA mismatch repair gene Mlh1 under hypoxic stress in mammalian cells. *Mol Cell Biol* 2003; 23:3265–73.
81. Rodríguez-Jiménez FJ, Moreno-Manzano V, Lucas-Dominguez R, Sánchez-Puelles J-M. Hypoxia causes downregulation of mismatch repair system and genomic instability in stem cells. *Stem Cells* 2008;26:2052–62.
82. Nakamura H, Tanimoto K, Hiyama K, Yunokawa M, Kawamoto T, Kato Y, et al. Human mismatch repair gene, MLH1, is transcriptionally repressed by the hypoxia-inducible transcription factors, DEC1 and DEC2. *Oncogene* 2008;27:4200–9.
83. Bindra RS, Gibson SL, Meng A, Westermarck U, Jasin M, Pierce AJ, et al. Hypoxia-induced down-regulation of BRCA1 expression by E2Fs. *Cancer Res* 2005;65:11597–604.
84. Bonneville R, Krook MA, Kautto EA, Miya J, Wing MR, Chen H-Z, et al. Landscape of microsatellite instability across 39 cancer types. *JCO Precis Oncol* 2017;2017:1–15.
85. Calsina B, Piñero-Yáñez E, Martínez-Montes ÁM, Caleiras E, Fernández-Sanromán Á, Monteagudo M, et al. Genomic and immune landscape of metastatic pheochromocytoma and paraganglioma. *Nat Commun* 2023;14:1122.
86. Sulkowski PL, Sundaram RK, Oeck S, Corso CD, Liu Y, Noorbakhsh S, et al. Krebs-cycle-deficient hereditary cancer syndromes are defined by defects in homologous-recombination DNA repair. *Nat Genet* 2018;50:1086–92.
87. Bechmann N, Poser I, Seifert V, Greunke C, Ullrich M, Qin N, et al. Impact of extrinsic and intrinsic hypoxia on catecholamine biosynthesis in absence or presence of Hif2 $\alpha$  in pheochromocytoma cells. *Cancers (Basel)* 2019;11:594.
88. Puchalska P, Crawford PA. Multi-dimensional roles of ketone bodies in fuel metabolism, signaling, and therapeutics. *Cell Metab* 2017;25:262–84.
89. Pajuelo Reguera D, Čunátová K, Vrbacký M, Pecinová A, Houštěk J, Mráček T, et al. Cytochrome c oxidase subunit 4 isoform exchange results in modulation of oxygen affinity. *Cells* 2020;9:443.
90. Fukuda R, Zhang H, Kim J-w, Shimoda L, Dang CV, Semenza GLL. HIF-1 regulates cytochrome oxidase subunits to optimize efficiency of respiration in hypoxic cells. *Cell* 2007;129:111–22.
91. Kastriiti ME, Faure L, Von Ahsen D, Boudierlique TG, Boström J, Solovieva T, et al. Schwann cell precursors represent a neural crest-like state with biased multipotency. *EMBO J* 2022;41:e108780.
92. Scortegagna M, Ding K, Oktay Y, Gaur A, Thurmond F, Yan LJ, et al. Multiple organ pathology, metabolic abnormalities and impaired homeostasis of reactive oxygen species in *Epas1*<sup>-/-</sup> mice. *Nat Genet* 2003;35:331–40.
93. Celada L, Cubiella T, San-Juan-guardado J, San José Martínez A, Valdés N, Jiménez-Fonseca P, et al. Differential HIF2 $\alpha$  protein expression in human carotid body and adrenal medulla under physiologic and tumorigenic conditions. *Cancers (Basel)* 2022;14:2986.
94. Arvanitaki A, Gatzoulis MA, Opatowsky AR, Khairy P, Dimopoulos K, Diller GP, et al. Eisenmenger syndrome: JACC state-of-the-art review. *J Am Coll Cardiol* 2022;79:1183–98.
95. Harris AL. Hypoxia—a key regulatory factor in tumour growth. *Nat Rev Cancer* 2002;2:38–47.
96. Vaupel P, Mayer A. Hypoxia in cancer: significance and impact on clinical outcome. *Cancer Metastasis Rev* 2007;26:225–39.
97. Lagercrantz H, Slotkin TA. The “stress” of being born. *Sci Am* 1986;254:100–7.
98. Takeuchi Y, Mochizuki-Oda N, Yamada H, Kurokawa K, Watanabe Y. Nonneurogenic hypoxia sensitivity in rat adrenal slices. *Biochem Biophys Res Commun* 2001;289:51–6.
99. Thompson RJ, Jackson A, Nurse CA. Developmental loss of hypoxic chemosensitivity in rat adrenomedullary chromaffin cells. *J Physiol* 1997;498:503–10.
100. Slotkin TA, Seidler FJ. Adrenomedullary catecholamine release in the fetus and newborn: secretory mechanisms and their role in stress and survival. *J Dev Physiol* 1988;10:1–16.
101. Tarade D, Robinson CM, Lee JE, Ohh M. HIF-2 $\alpha$ -pVHL complex reveals broad genotype-phenotype correlations in HIF-2 $\alpha$ -driven disease. *Nat Commun* 2018;9:3359.
102. Jeong C, Witonsky DB, Basnyat B, Neupane M, Beall CM, Childs G, et al. Detecting past and ongoing natural selection among ethnically Tibetan women at high altitude in Nepal. *PLoS Genet* 2018; 14:e1007650.
103. Beall CM, Song K, Elston RC, Goldstein MC. Higher offspring survival among Tibetan women with high oxygen saturation genotypes residing at 4,000 m. *Proc Natl Acad Sci U S A* 2004;101:14300–4.
104. He Y, Guo Y, Zheng W, Yue T, Zhang H, Wang B, et al. Polygenic adaptation leads to a higher reproductive fitness of native Tibetans at high altitude. *Curr Biol* 2023;33:4037–51.e5.
105. Diaz RJ. Overview of hypoxia around the world. *J Environ Qual* 2001;30:275–81.
106. Oldenburg O, Wellmann B, Buchholz A, Bitter T, Fox H, Thiem U, et al. Nocturnal hypoxaemia is associated with increased mortality in stable heart failure patients. *Eur Heart J* 2016;37:1695–703.
107. Ozeke O, Ozer C, Gungor M, Celenk MK, Dincer H, Ilicin G. Chronic intermittent hypoxia caused by obstructive sleep apnea may play an important role in explaining the morbidity-mortality paradox of obesity. *Med Hypotheses* 2011;76:61–3.
108. Ramachandrapa A, Rosenberg ES, Wagoner S, Jain L. Morbidity and mortality in late preterm infants with severe hypoxic respiratory failure on extra-corporeal membrane oxygenation. *J Pediatr* 2011;159:192–8.e3.
109. Adeloje D, Song P, Zhu Y, Campbell H, Sheikh A, Rudan I, et al. Global, regional, and national prevalence of, and risk factors for, chronic obstructive pulmonary disease (COPD) in 2019: a systematic review and modelling analysis. *Lancet Respir Med* 2022;10:447–58.
110. Tremblay JC, Ainslie PN. Global and country-level estimates of human population at high altitude. *Proc Natl Acad Sci U S A* 2021;118:e2102463118.
111. Hoffman JIE, Kaplan S. The incidence of congenital heart disease. *J Am Coll Cardiol* 2002;39:1890–900.
112. Lee S, Nakamura E, Yang H, Wei W, Linggi MS, Sajan MP, et al. Neuronal apoptosis linked to EglN3 prolyl hydroxylase and familial pheochromocytoma genes: developmental culling and cancer. *Cancer Cell* 2005;8:155–67.
113. Eckardt L, Prange-Barczynska M, Hodson EJ, Fielding JW, Cheng X, Lima JDCC, et al. Developmental role of PHD2 in the pathogenesis of pseudohypoxic pheochromocytoma. *Endocr Relat Cancer* 2021;28:757–72.
114. Burton GJ, Cindrova-Davies T, Yung HW, Jauniaux E. Hypoxia and reproductive health: oxygen and development of the human placenta. *Reproduction* 2021;161:F53–65.
115. West JB, Hackett PH, Maret KH, Milledge JS, Peters RM, Pizzo CJ, et al. Pulmonary gas exchange on the summit of Mount Everest. *J Appl Physiol Respir Environ Exerc Physiol* 1983;55:678–87.
116. Grocott MPW, Martin DS, Levett DZH, McMorrow R, Windsor J, Montgomery HE, et al. Arterial blood gases and oxygen content in climbers on Mount Everest. *N Engl J Med* 2009;360:140–9.
117. Macias D, Cowburn AS, Torres-Torreal H, Ortega-Sáenz P, López-Barneo J, Johnson RS. HIF-2 $\alpha$  is essential for carotid body development and function. *Elife* 2018;7:e34681.
118. Colinas O, Moreno-Domínguez A, Ortega-Sáenz P, López-Barneo J. Constitutive expression of Hif2 $\alpha$  confers acute O<sub>2</sub> sensitivity to carotid body glomus cells. *Adv Exp Med Biol* 2023;1427:153–62.
119. Jain IH, Zazzeron L, Goli R, Alexa K, Schatzman-Bone S, Dhillon H, et al. Hypoxia as a therapy for mitochondrial disease. *Science* 2016;352:54–61.
120. Khazal F Al, Holte MN, Bolon B, White TA, LeBrasseur N, Iii LJM. A conditional mouse model of complex II deficiency manifesting as Leigh-like syndrome. *FASEB J* 2019;33:13189–201.
121. Niemann S, Müller U. Mutations in SDHC cause autosomal dominant paraganglioma, type 3. *Nat Genet* 2000;26:268–70.
122. Kamihara J, Hamilton KV, Pollard JA, Clinton CM, Madden JA, Lin J, et al. Belzutifan, a potent HIF2 $\alpha$  inhibitor, in the pacak-Zhuang syndrome. *N Engl J Med* 2021;385:2059–65.

123. Alkaiissi H, Nazari MA, Hadrava Vanova K, Uher O, Gordon CM, Talvacchio S, et al. Rapid cardiovascular response to belzutifan in HIF2A-mediated paraganglioma. *N Engl J Med* 2024;391:1552–5.
124. Warnes CA, Liberthson R, Danielson GK, Dore A, Harris L, Hoffman JI, et al. Task force 1: the changing profile of congenital heart disease in adult life. *J Am Coll Cardiol* 2001;37:1170–5.
125. Lenders JWM, Duh QY, Eisenhofer G, Gimenez-Roqueplo AP, Grebe SKG, Murad MH, et al. Pheochromocytoma and paraganglioma: an endocrine society clinical practice guideline. *J Clin Endocrinol Metab* 2014;99:1915–42.
126. Benjamini Y, Hochberg Y. Controlling the false discovery rate: a practical and powerful approach to multiple testing. *J R Stat Soc Ser B (Methodol)* 1995;57:289–300.
127. Cerami E, Gao J, Dogrusoz U, Gross BE, Sumer SO, Aksoy BA, et al. The cBio cancer genomics portal: an open platform for exploring multi-dimensional cancer genomics data. *Cancer Discov* 2012;2:401–4.
128. de Bruijn I, Kundra R, Mastrogiacomo B, Tran TN, Sikina L, Mazor T, et al. Analysis and visualization of longitudinal genomic and clinical data from the AACR project GENIE biopharma collaborative in cBioPortal. *Cancer Res* 2023;83:3861–7.
129. Van der Auwera GA, Carneiro MO, Hartl C, Poplin R, del Angel G, Levy-Moonshine A, et al. From FastQ data to high confidence variant calls: the Genome Analysis Toolkit best practices pipeline. *Curr Protoc Bioinformatics* 2013;43:11.10.1–33.
130. Karczewski KJ, Francioli LC, Tiao G, Cummings BB, Alfoldi J, Wang Q, et al. The mutational constraint spectrum quantified from variation in 141,456 humans. *Nature* 2020;581:434–43.
131. Karczewski KJ, Weisburd B, Thomas B, Solomonson M, Ruderfer DM, Kavanagh D, et al. The ExAC browser: displaying reference data information from over 60 000 exomes. *Nucleic Acids Res* 2017;45:D840–5.
132. Van Loo P, Nordgard SH, Lingjærde OC, Russnes HG, Rye IH, Sun W, et al. Allele-specific copy number analysis of tumors. *Proc Natl Acad Sci U S A* 2010;107:16910–5.
133. Ewels PA, Peltzer A, Fillinger S, Patel H, Alneberg J, Wilm A, et al. The nf-core framework for community-curated bioinformatics pipelines. *Nat Biotechnol* 2020;38:276–8.
134. Garcia M, Juhos S, Larsson M, Olason PI, Martin M, Eisfeldt J, et al. Sarek: a portable workflow for whole-genome sequencing analysis of germline and somatic variants. *F1000Res* 2020;9:63.
135. Hanssen F, Garcia MU, Folkersen L, Pedersen AS, Lescai F, Jodoin S, et al. Scalable and efficient DNA sequencing analysis on different compute infrastructures aiding variant discovery. *NAR Genom Bioinform* 2024;6:lqae031.
136. Alexandrov LB, Ju YS, Haase K, Van Loo P, Martincorena I, Nik-Zainal S, et al. Mutational signatures associated with tobacco smoking in human cancer. *Science* 2016;354:618–22.
137. Grigoriadis K, Huebner A, Bunkum A, Colliver E, Frankell AM, Hill MS, et al. CONIPHER: a computational framework for scalable phylogenetic reconstruction with error correction. *Nat Protoc* 2023;19:159–83.
138. Li H, Durbin R. Fast and accurate short read alignment with Burrows–Wheeler transform. *Bioinformatics* 2009;25:1754–60.
139. Van der Auwera GA, O'Connor BD. Genomics in the cloud: Using docker, GATK, and WDL in terra. Sebastopol (CA): O'Reilly Media, Inc.; 2020. p. 493–502.
140. Cibulskis K, Lawrence MS, Carter SL, Sivachenko A, Jaffe D, Sougnez C, et al. Sensitive detection of somatic point mutations in impure and heterogeneous cancer samples. *Nat Biotechnol* 2013;31:213–9.
141. McLaren W, Gil L, Hunt SE, Riat HS, Ritchie GRS, Thormann A, et al. The Ensembl variant effect predictor. *Genome Biol* 2016; 17:122.
142. Kautto EA, Bonneville R, Miya J, Yu L, Krook MA, Reeser JW, et al. Performance evaluation for rapid detection of pan-cancer microsatellite instability with MANTIS. *Oncotarget* 2017;8:7452–63.
143. Shen R, Seshan VE. FACETS: allele-specific copy number and clonal heterogeneity analysis tool for high-throughput DNA sequencing. *Nucleic Acids Res* 2016;44:e131.
144. Ellrott K, Bailey MH, Saksena G, Covington KR, Kandath C, Stewart C, et al. Scalable open science approach for mutation calling of tumor exomes using multiple genomic pipelines. *Cell Syst* 2018;6:271–81.e7.
145. Weghorn D, Sunyaev S. Bayesian inference of negative and positive selection in human cancers. *Nat Genet* 2017;49:1785–8.
146. Love MI, Huber W, Anders S. Moderated estimation of fold change and dispersion for RNA-seq data with DESeq2. *Genome Biol* 2014; 15:550.
147. Richter S, D'Antongiovanni V, Martinelli S, Bechmann N, Rivero M, Poitz DM, et al. Primary fibroblast co-culture stimulates growth and metabolism in Sdhb-impaired mouse pheochromocytoma MTT cells. *Cell Tissue Res* 2018;374:473–85.
148. Richter S, Geldon L, Pang Y, Peitzsch M, Huynh T, Leton R, et al. Metabolome-guided genomics to identify pathogenic variants in isocitrate dehydrogenase, fumarate hydratase, and succinate dehydrogenase genes in pheochromocytoma and paraganglioma. *Genet Med* 2019;21:705–17.
149. Picelli S, Björklund ÅK, Faridani OR, Sagasser S, Winberg G, Sandberg R. Smart-seq2 for sensitive full-length transcriptome profiling in single cells. *Nat Methods* 2013;10:1096–100.
150. Greene LA, Tischler AS. Establishment of a noradrenergic clonal line of rat adrenal pheochromocytoma cells which respond to nerve growth factor. *Proc Natl Acad Sci U S A* 1976;73:2424–8.
151. Hopewell R, Ziff EB. The nerve growth factor-responsive PC12 cell line does not express the Myc dimerization partner Max. *Mol Cell Biol* 1995;15:3470–8.
152. O'Driscoll CM, Gorman AM. Hypoxia induces neurite outgrowth in PC12 cells that is mediated through adenosine A2A receptors. *Neuroscience* 2005;131:321–9.
153. Chen S, Zhou Y, Chen Y, Gu J. fastp: an ultra-fast all-in-one FASTQ preprocessor. *Bioinformatics* 2018;34:i884–90.
154. Patro R, Duggal G, Love MI, Irizarry RA, Kingsford C. Salmon provides fast and bias-aware quantification of transcript expression. *Nat Methods* 2017;14:417–9.
155. Sonesson C, Love MI, Robinson MD. Differential analyses for RNA-seq: transcript-level estimates improve gene-level inferences. *F1000Research* 2015;4:1521.
156. Young MD, Wakefield MJ, Smyth GK, Oshlack A. Gene ontology analysis for RNA-seq: accounting for selection bias. *Genome Biol* 2010;11:R14.
157. Subramanian A, Tamayo P, Mootha VK, Mukherjee S, Ebert BL, Gillette MA, et al. Gene set enrichment analysis: a knowledge-based approach for interpreting genome-wide expression profiles. *Proc Natl Acad Sci U S A* 2005;102:15545–50.
158. Espina M, Corte-Rodríguez M, Aguado L, Montes-Bayón M, Sierra MI, Martínez-Cambor P, et al. Cisplatin resistance in cell models: evaluation of metallomic and biological predictive biomarkers to address early therapy failure. *Metallomics* 2017;9:564–74.